A Novel Trajectory Vector Approach for Characterizing Dynamic Changes in the Performance-Load Representation of Cardiac State

by

Julie Shen

B.S., University of California, Berkeley (2020)

Submitted to the Department of Mechanical Engineering
in partial fulfillment of the requirements for the degree of

Master of Science in Mechanical Engineering

at the

MASSACHUSETTS INSTITUTE OF TECHNOLOGY

May 2022

Author .....
Department of Mechanical Engineering
May 6, 2022

Certified by .....
Elazer R. Edelman
Edward J. Poitras Professor, Medical Engineering and Science
Thesis Supervisor

Accepted by .....
Nicolas Hadjiconstantinou
Professor, Graduate Officer

A Novel Trajectory Vector Approach for Characterizing Dynamic Changes in the Performance-Load Representation of Cardiac State

by

Julie Shen

Submitted to the Department of Mechanical Engineering
on May 6, 2022, in partial fulfillment of the
requirements for the degree of
Master of Science in Mechanical Engineering

Abstract

In this work, we present a novel trajectory vector approach to both qualitatively and quantitatively characterize dynamic changes in the performance-load cardiac relationship for application in the context of cardiogenic shock. The performance-load relationship is an expansion on the Frank-Starling mechanism that allows traditional metrics of preload to be correlated with afterload, combining both types of load into a more comprehensive general cardiac load. Through a series of controlled animal studies, we collect hemodynamic data during baseline and various pharmacological interventions while the animal is supported by a percutaneous ventricular assist device to test the feasibility of this approach. Utilizing a 2D Frank-Starling representation of the hemodynamic animal data, we employ Gaussian mixture model clustering to identify distinct patterns in an animal's drug response. These patterns guide the formulation of trajectory vectors, parameterized by angle and magnitude, for each drug effect. Feasibility of the trajectory vector approach is validated through confirming the independence of angle and magnitude from baseline state. The ability of the approach to detect changes across a spectrum of distinct cardiac states and distinguish intervention dose levels, with minimal influences from the level of Impella support, is realized. With the ability to monitor shifts in performance-load relationship, a reflection of the heart's current inotropic state, our technique can be applied in the clinic to inform appropriate pharmacological treatment and device management for patients with cardiogenic shock.

Thesis Supervisor: Elazer R. Edelman
Title: Edward J. Poitras Professor, Medical Engineering and Science

Acknowledgments

First and foremost, I would like to acknowledge my advisor, Dr. Elazer Edelman, for his constant encouragement and guidance during the development of this work. He has always offered his warmth and welcome to make me feel supported, despite the unique circumstances surrounding my transition into MIT. As I look toward moving onto the PhD program, I express my deepest gratitude to Elazer for inspiring my continual growth as a researcher.

I would also like to thank my fellow colleagues in the Edelman Lab, especially Dr. Steven Keller and Dr. Brian Chang, who served as my mentors during the formulation of this work and contributed significantly to the groundwork for this project. Thank you to Efi Goffer and Kim Lamberti for their constant support since I joined the mechanical circulatory support subgroup.

I would like to acknowledge the colleagues and researchers at Abiomed, Inc. for enabling this work. Their collaboration allowed me to explore a multitude of opportunities in my research.

Lastly, I would like to thank my family for their unconditional support of my pursuit of higher education. I would not be where I am today if it weren't for their continual encouragement and admirable work ethic.

Contents

List of Figures

List of Tables

List of Acronyms and Terms

ACE angiotensin-converting enzyme

AIC Akaike information criterion

BIC Bayesian information criterion

CO cardiac output

CS cardiogenic shock

DBSCAN density-based spatial clustering of applications with noise

ECMO extracorporeal membrane oxygenation

EDP end-diastolic pressure

EDV end-diastolic volume

EKG electrocardiogram

ESPVR end-systolic pressure-volume relationship

F-S Frank-Starling

GMM Gaussian mixture model

IABP intra-aortic balloon pump

IV intravenous

IVC inferior vena cava

LV left ventricular

MAP mean arterial pressure

MAP-DP maximum a-posteriori Dirichlet process mixtures

MCS mechanical circulatory support

P-L performance-load

PAC pulmonary artery catheter

PCWP pulmonary capillary wedge pressure

PV pressure-volume

pVAD percutaneous ventricular assist device

PVC premature ventricular contraction

QRS complex a combination of the Q, R, and S waves in an electrocardiogram signal

RR interval time elapsed between two successive R waves in an electrocardiogram signal

SV stroke volume

SvO2 mixed venous oxygen saturation

SVR systemic vascular resistance

Chapter 1

Introduction

Cardiogenic shock (CS) is the condition in which cardiac work produced is insufficient to meet the metabolic needs of the body. It often leads to end-organ hypoperfusion, which can progress to become life-threatening. CS is classically characterized by low cardiac output and high filling pressures. The incidence of cardiogenic shock has been increasing in recent years and mortality remains high [1][2]. Current treatments include pharmacological interventions to improve cardiac performance and mechanical circulatory support (MCS) devices, which help assist native heart function when it is inadequate [3].

Clinicians often rely on hemodynamic measurements from catheters to help titrate treatment. Particularly, certain hemodynamic measurements can characterize the Frank-Starling (F-S) relationship, which is often used to assess cardiac function. The F-S relationship explains an important mechanism in cardiovascular physiology, in which the amount of ventricular filling, or preload on the heart, affects the ability of the ventricle to contract, which in turn influences cardiac output, a measure of cardiac performance. This relationship can be depicted as a curve with preload as the independent variable, measured as end-diastolic volume (EDV) or end-diastolic pressure (EDP), and cardiac performance as the dependent variable, measured as stroke volume (SV) or cardiac output (CO) (Figure 1-1) [4]. The curve reflects the heart's current inotropic, or contractile, state and shifts in this curve, influenced by changes in contractility and vascular tone, can be used to see how a patient is

progressing or regressing. For instance, the onset of heart failure shifts the curve downward, as the heart can no longer maintain its usual cardiac output at the same filling pressure (Figure 1-1).

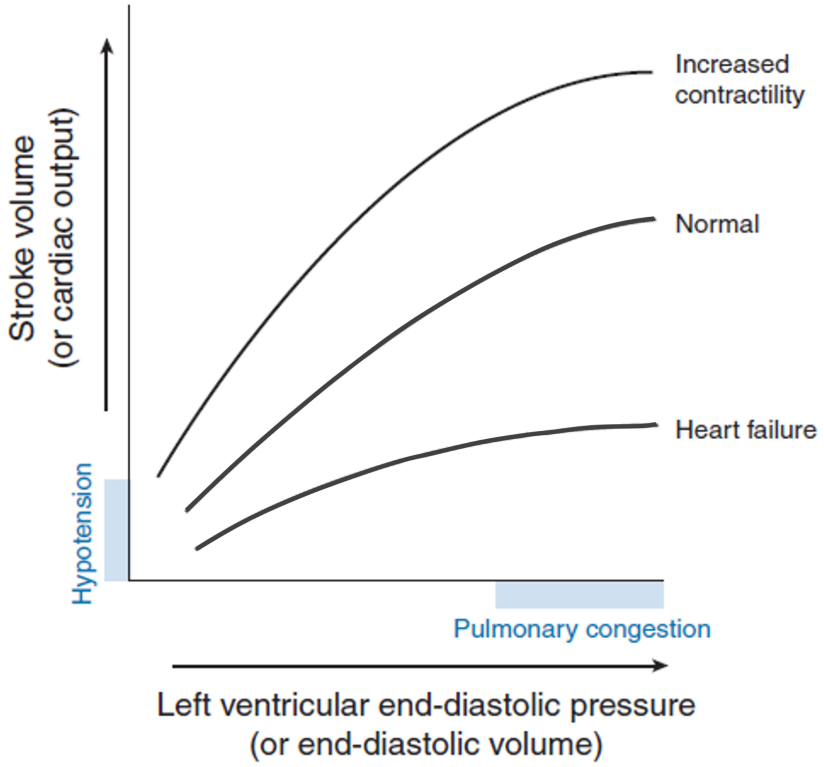

Figure 1-1: Frank-Starling curves relate preload to cardiac performance. Preload is measured as left ventricular end-diastolic pressure (LVEDP) or end-diastolic volume (LVEDV), and cardiac performance is measured as stroke volume (SV) or cardiac output (CO). The curve of a normal heart displays a positively increasing cardiac performance as a function of preload. At a state of increased contractility, cardiac performance is augmented at similar preload. For a curve representing heart failure, decreased contractility shifts the normal curve downward. Adapted from *Pathophysiology of Heart Disease*, Fifth Edition by L.S. Lilly [4].

The pulmonary artery catheter (PAC) is the most commonly used device for measuring a variety of hemodynamic metrics [5]. Through the PAC, pulmonary capillary wedge pressure (PCWP) can be used to derive left ventricular EDP (LVEDP), and oxygen saturation or thermodilution can be used to derive CO. Although one of the most common methods to monitor patient hemodynamics, PAC use has been declining in recent years with increased appreciation of the risk of insertion and little

benefit to clinical outcomes [6][7][8][9]. According to current guidelines, PAC use is limited to patients with CS or mechanical ventilation, and not recommended for routine management of heart failure [10]. Limitations of the PAC include intermittent data sampling (e.g. PCWP) [11], oversimplification of parameters (fixed and linear systemic vascular resistance, or SVR), and complications with insertion [12].

In addition to the lack of beneficial hemodynamic monitoring tools, accessible metrics are of limited value in directing care of cardiogenic shock. The complexity of this condition makes it difficult for a generalized hemodynamic target to guide its treatment. There are no well-established hemodynamic targets for patients with CS, specifically suggestions for mean arterial pressure (MAP) or systolic blood pressure (SBP) [13]. As such, just as underlying physiology varies from patient to patient, hemodynamic target metrics must also be individualized for optimal management of CS.

Recent innovation in the management of CS can be seen in the variety of MCS devices that are currently used to treat and manage cardiogenic shock, categorized as short-term or long-term. This work focuses on short-term devices, which provide temporary support for patients during high-risk procedures or those awaiting more definitive prognosis and treatment. The current landscape is comprised of percutaneous ventricular assist devices (pVADs), which generally alleviate high blood pressures and/or improve cardiac output. The most commonly used are the intra-aortic balloon pump (IABP), extracorporeal membrane oxygenation (ECMO), the Impella® pump, and the TandemHeart® pump [13]. Unfortunately, there are mixed outcomes associated with the use of pVADs, with limited evidence to support the use of these devices in patients with cardiogenic shock. However, while the use of the traditional IABP has been seen to significantly decrease, the use of the more contemporary Impella CP has become more frequent in recent years [14][15]. The rise of this heart pump shows promise in its utility for managing CS, provided selection of the appropriate patient case.

Percutaneous ventricular assist devices have the potential to simultaneously (1) maintain systemic perfusion and support native cardiac function and (2) provide

hemodynamic monitoring of dynamic cardiac state. By directly and locally assessing heart-device interactions in real-time and continuously, pVADs can inform clinicians about the current state of the cardiovascular system, future management of the device, and individualized treatment options. Due to these reasons, these devices can become better alternatives to pulmonary artery catheters. Additionally, using pVADs to monitor patient state eliminates the need for extra indwelling monitoring devices, thereby reducing patient risk, lowering clinical costs, and improving patient recovery.

In particular, utilizing the Impella CP to monitor patient state can provide valuable insight into both ventricular-vascular interaction, such as the Frank-Starling relationship depicts, and device-heart interaction, as the pump continuously supports the patient. The Impella CP is an intravascular microaxial pump that supports a patient's circulatory system by delivering blood from the left ventricle into the ascending aorta [16]. In previous work, it was discovered that intrinsic device parameters of the Impella CP can be used to determine the critical metrics of LVEDP [17] and CO [18]. When compared to the gold standard metrics measured from PCWP and thermodilution, the hysteresis-derived LVEDP and algorithm-determined CO were closely correlated ($R^2 = 0.96$ and $r = 0.82$ respectively). Using these prior methods to calculate LVEDP and CO from the Impella CP, we may be able to observe any dynamic changes in real-time, continuous fashion to inform clinicians about patient condition.

We propose a novel trajectory vector approach used in the context of a performance-load (P-L) relationship to differentiate significant cardiac events from naturally occurring variability. Rather than portraying the classical Frank-Starling mechanism which is described by cardiac performance and preload, here we establish a general performance-load relationship. By relying on the metric of LVEDP, a measure of preload, to detect changes in vascular tone, which directly affects afterload, we can broaden characterization of preload to a more complex variable that integrates all cardiac load. A trajectory vector, parameterized by a direction and magnitude, can define how a patient's inotropic state is moving from one point to another, in the form of shifts in the P-L relationship. For example, for a patient undergoing heart failure, the downward shift of the P-L relationship could now be depicted by the green

arrow in Figure 1-2. The range of patient responses to a particular cardiac event or intervention could be reflected by the corresponding colored region. Once this trajectory is established between a previous state and the current state, it may be used to predict trends in moving patient state. Trajectories established for particular pharmacological interventions that directly influence the performance-load relationship, such as inotropic and vasoactive drugs, can guide pharmacological treatment. During Impella support, trajectories can also guide device management, such as titrating support level and determining weaning.

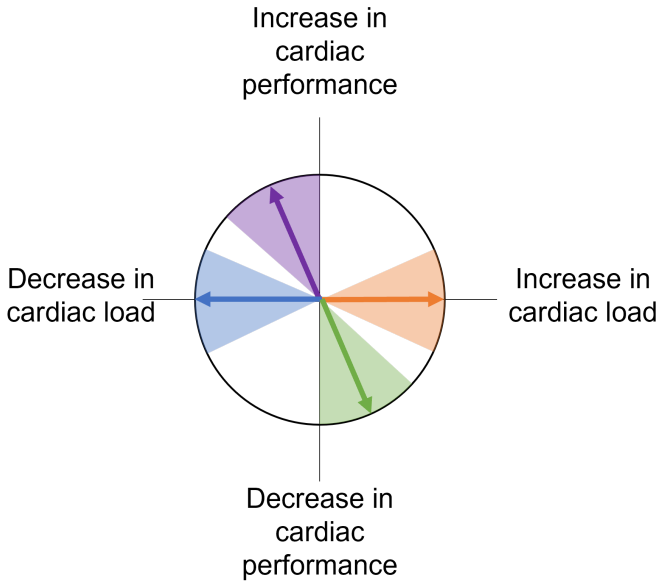

Figure 1-2: Trajectory vectors depicting shifts in the Frank-Starling curve. The purple and green regions correlate with increased and decreased contractility respectively. The orange and blue regions correlate with increased and decreased vascular tone respectively.

Currently, clinicians rely on hemodynamic monitoring in the form of separate metrics, such as MAP or CO, to guide treatment of CS. However, changes within individual metrics over time may be hard to interpret. Fluctuations in the signal could be caused by significant phenomenon or just due to local variability. Rather than a one-dimensional metric, a combination of two metrics over the same time scale, such as that represented by the performance-load relationship, may provide better resolution of changes in patient state.

As mentioned previously, cardiogenic shock mortality and incidence still remain high, even with recent innovation of device technology for treatment. These trends are likely due to poor understanding of an individual patient's underlying physiology, which is imperative to guide proper treatment and establish tailored target metrics. Even with the higher resolution Frank-Starling representation, the movement along an F-S curve is dependent on said curve, or the current state of the heart. This reliance on prior patient state poses a challenge with using the Frank-Starling relationship as a generalized monitoring and diagnostic metric for the heterogeneous condition of CS. However, the trajectory vector approach, which we hypothesize to be independent of baseline state, has the potential to track relative changes without relying on knowledge of a patient's underlying physiology. This possible state independence has profound impact on the clinical utility of this metric due to repeatable characterization of an assortment of patient states.

We aim to define a means of depicting dynamic changes in the performance-load (P-L) relationship in real-time, which has the potential to predict the trajectory of a patient's cardiac state using the Impella CP's intrinsic parameters. We propose three key questions regarding the trajectory vector approach:

1. Can a trajectory vector approach be used to estimate shifts in the P-L relationship?

2. Can we use Impella-derived metrics to characterize these trends?

3. Can this approach be used to predict the trajectory of changing cardiac behavior?

This work primarily focuses on addressing the first question, proving the feasibility of the proposed metric and approach. Validation of this approach is achieved through the continuous monitoring of the progression of cardiac state in a controlled series of animal studies using the Impella CP, the application of clustering analysis to identify patterns in data, and the establishment of trajectory vectors between the observed cardiac states, spanning the range of existing performance-load relationship shifts as

represented by the four quadrants in Figure 1-2. Through the qualitative visualization of a patient's changing inotropic state regardless of their prior state and quantitative metrics defined by trajectory angle and magnitude, clinicians may only need to rely on a singular pVAD to simultaneously monitor and treat a patient.

Chapter 2

Exploration of Animal Hemodynamic Data

A general method was defined for developing the trajectory vector approach and ensuring the approach's feasibility, which can be comprised by a series of aims. Specifically, the first aim was to perform a controlled study on an animal supported by the Impella to collect reliable hemodynamic data during a range of physiological states. The second aim was to analyze the hemodynamic data during the various states in a 2D performance-load representation. The third and final aim was to identify any dynamic changes from one state to another using statistical methods and utilize the trajectory vector approach to characterize these changes. This chapter details the process taken to explore a series of animal studies previously conducted and use the resulting collected data to develop analytic techniques.

2.1 Analysis of previous animal studies

Data from prior animal studies were used to build and refine my analytic approach. In a series of animal studies conducted in 2020, the Yorkshire pig was used as both a healthy and an acute cardiogenic shock model while on Impella device support. Hemodynamic data was collected during the baseline of the healthy model, five different drug-impacted states of the healthy model, and the baseline of the acute model.

2.1.1 VBU00141: Animal study data from August 2020

The first study of the series, designated as VBU00141, was the subject of initial data analysis techniques. The first objective with this data was to perform continuous hemodynamic data analysis, in which left ventricular end-diastolic pressure and cardiac output were viewed to change over time from the beginning of a state's baseline to the end of a steady-state drug effect. Two minutes of baseline data and ten minutes of drug effect data were analyzed. Taking a moving average across this joint section of data allowed any physiological changes lying within the reference measurements to be detected. In addition to evaluating the hemodynamic metrics separately, LVEDP and CO were plotted together against time to observe how the P-L relationship shifted while an intervention occurred. Across the joint section of data, beat-to-beat movement along the Frank-Starling curve[1] and the transition points between the baseline before drug administration and steady-state drug effect could be observed (Figure 2-1). Based on these findings, relying on isolated data points is insufficient for differentiating state changes, and dynamic illustration is required for capturing state transitions.

Additionally, the difference between using reference measurements from indwelling catheters and using inferred measurements from the Impella device was explored, particularly regarding the pressure signals. The differentiation of cardiac states within healthy and acute models was examined on a Frank-Starling plot (Figure 2-2). The drug responses observed were standardized using z-score standardization to their respective baselines to allow comparison between differing baselines and across multiple units of measure. It was discovered that detecting distinct states is difficult when solely utilizing beat-to-beat data points, as points from different drug effects often overlapped. A statistical model to quantitatively separate varying distributions within an overall data set may be more helpful to track different state changes.

With the data standardized and grouped by animal state (i.e. baseline or drug

[1] Although the eventual context surrounding the trajectory vector approach is based on a broad performance-load relationship, in this work we still rely on the analysis of metrics of LVEDP and CO that traditionally outline the Frank-Starling curve.

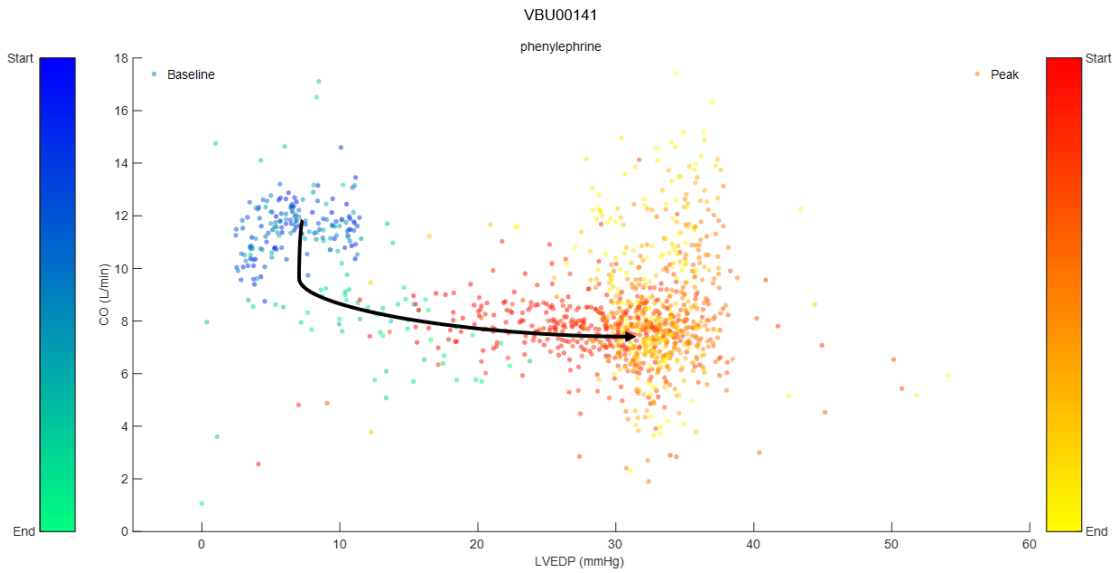

Figure 2-1: Beat-to-beat points placed on a Frank-Starling plot. For animal study VBU00141, two minutes of baseline data and ten minutes of drug effect data were observed during the administration of phenylephrine. The gradient bars indicate the span of baseline and peak drug effect. The arrow indicates the transition from baseline to steady-state drug effect.

effect), circular clusters with radii equivalent to two z-scores were superimposed onto the data groups as a simplification of the previously suggested statistical model (Figure 2-3). The centers of these fixed clusters were defined using the centroids of the data groups, corresponding to the means of both the LVEDP and CO metrics. Two z-scores were chosen for the radii since data falling within two standard deviations from the mean for a normal distribution should encompass 95% of the data set, a common standard used in statistical analysis. These manually affixed circles helped visually distinguish one state from another. Subsequently, vectors were drawn between the centroids of the clusters to quantitatively characterize the trajectory of how a particular baseline state transitioned to a steady-state drug state. These vectors, delineated by direction and magnitude, were also scaled to be of unit length to easily visualize their directions on a unit circle plot (Figure 2-4).

Figure 2-2: States of a healthy and acute cardiogenic shock model displayed in a Frank-Starling plot. For animal study VBU00141, the baseline prior to each intervention was evaluated. Interventions include phenylephrine (phenyl), dobutamine (dobut), epinephrine (epi), dobutamine during CS (shock dobut), and epinephrine during CS (shock epi). Detecting distinct states is difficult when solely utilizing beat-to-beat data points, as points from different drug effects often overlapped.

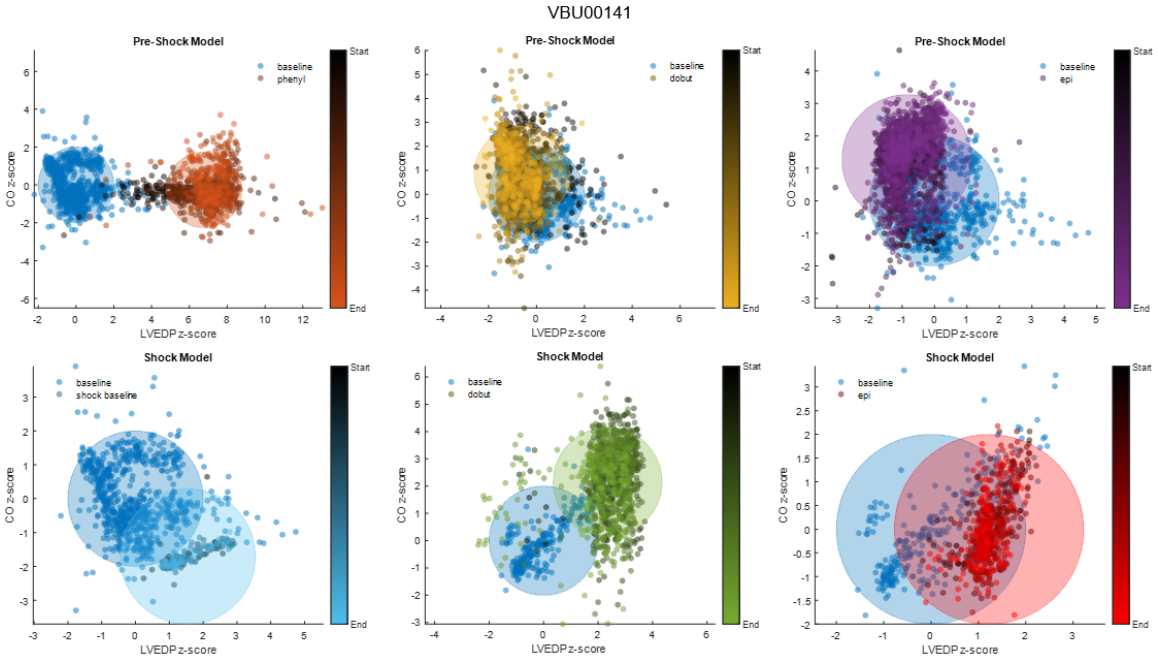

Figure 2-3: Standardization of points grouped by fixed clusters on a Frank-Starling plot. For animal study VBU00141, each intervention was standardized via z-score to its corresponding baseline. Clusters of radii equivalent to two z-scores were superimposed onto each state. The gradient bars indicate the span of peak drug effect, equivalent to ten minutes. Normalizing drug responses using z-score standardization to their respective baselines allows comparison between differing baselines and across multiple units of measure. Using manually affixed circles helps visually distinguish one state from another.

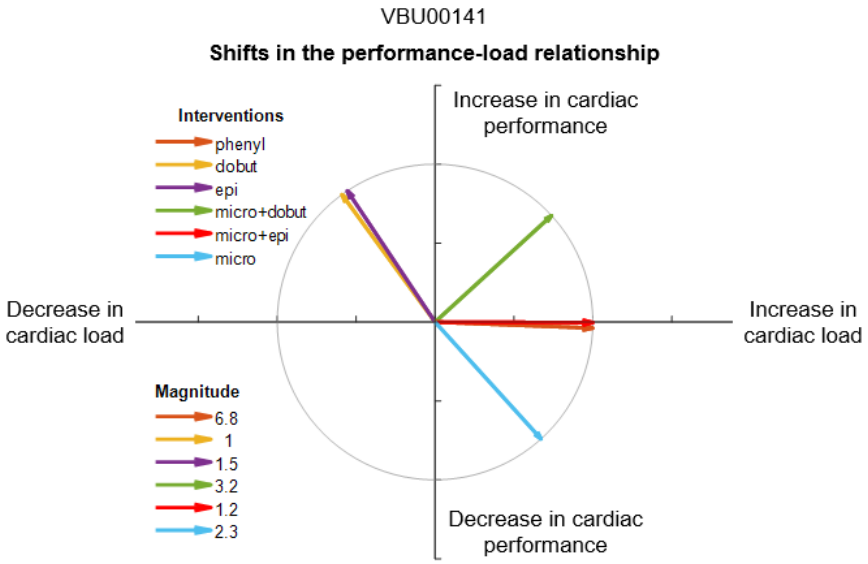

Figure 2-4: Trajectory vectors for interventions representing shifts in the performance-load relationship. For animal study VBU00141, trajectory vectors of unit length were generated for each intervention in a healthy and acute cardiogenic shock model. Interventions include phenylephrine (phenyl), dobutamine (dobut), epinephrine (epi), dobutamine during CS (micro+dobut), epinephrine during CS (micro+epi), and CS (micro). Vector magnitudes were also calculated.

2.1.2 VBU00148: Animal study data from November 2020

With the next study of the 2020 series, designated as VBU00148, the hope was to improve upon the previously established initial data analysis techniques. Some of these revisions included filtering of the raw data and incorporating data clustering, rather than fixed superimposition, to find patterns for the trajectory vector method. Furthermore, a few general challenges associated with analyzing sets of cardiovascular data were identified, such as the variability present in hemodynamic measurements.

One focus of this second iteration of analysis was on implementing clustering to more effectively separate varying distributions within an overall data set for tracking different state changes. Cluster analysis is a common statistical method where inferences are drawn from data sets to find hidden patterns in data that is unlabeled. Based on certain metrics, the unlabeled data set can be grouped into clusters, in which points from the same cluster have similar attributes and are distinct from points that belong to different clusters. I chose to start with density-based spatial clustering of applications with noise (DBSCAN) method, a simple and straightforward method which identifies arbitrarily shaped clusters and outliers in data based on density [19]. A data point is identified as part of a cluster if its surrounding neighborhood range, defined by a parameter ϵ, contains at least a minimum number of neighbors, defined by a parameter *minpts* (Figure 2-5).

There are several advantages with using clustering instead of manually fixing groups onto the data. With clustering, the amount of variability seen in pattern identification is reduced. Although there is much variability when looking at sections of data during different time points, clustering can be a reliable way to identify the same patterns with some amount of tolerance. For example, the clustering model may not identify an increase of 5 mmHg from the baseline LVEDP as an unusual change, but may pick up on an increase of 10 mmHg as indicative of a significant cardiac event. Most importantly, in a clinical setting, when a patient is remotely monitored, the exact timing and behavior of cardiac events may not be well understood, but with the use of cluster analysis, unknown dynamic changes within patient state can

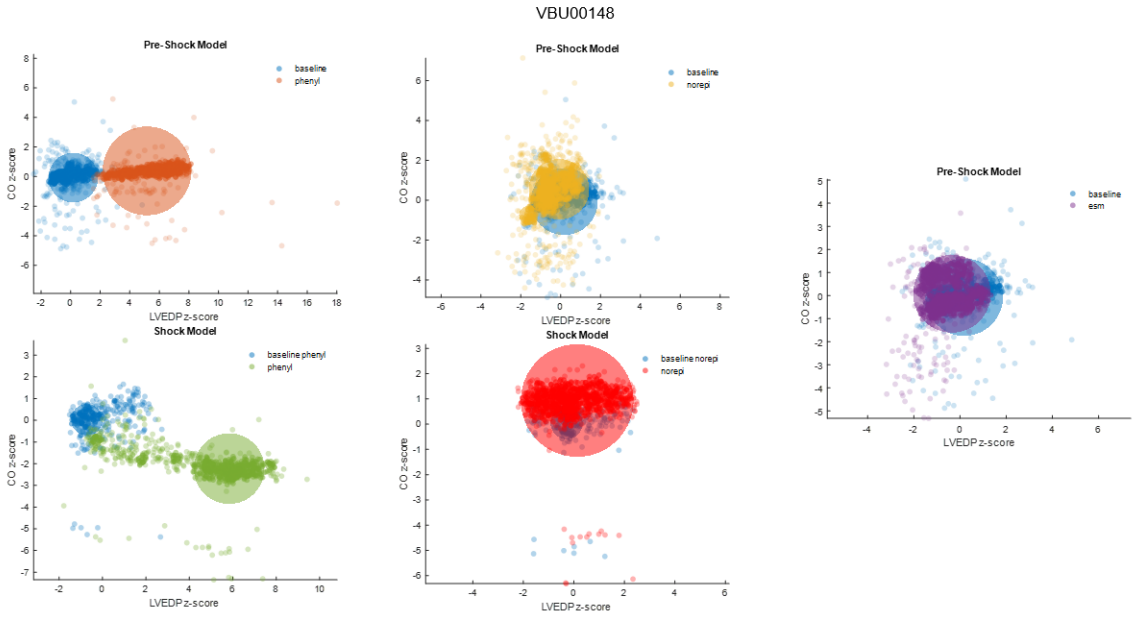

Figure 2-5: DBSCAN applied to Frank-Starling data from VBU00148. Clusters for each intervention and its corresponding baseline were identified. Unlike the clusters with fixed radii, clusters using DBSCAN have varied radii dependent on the density of the grouped points. This allows more flexibility in identifying differing distributions and patterns.

be detected over stretches of time. Once the parameters of the chosen clustering method are refined, uncharacterized events should be easily identified.

Multiple challenges arose when trying to improve upon data analytics. For one, different physiological behaviors expressed by the animal introduced variation in the observed physiological response to the pharmacological interventions. This variation made it difficult to accurately extract cardiac patterns with my data analysis techniques. For example, irregular rhythms and morphology in the electrocardiogram (EKG) signal would lead to overestimations of the animal's heart rate (Figure 2-6). With respiratory variation, in which the phasing of the respiratory cycle affects changes in blood pressure [20], large spread can be seen across both LVEDP and CO, making it difficult to differentiate actual physiological phenomenon from the typical variation that can be excluded. To improve the accuracy of my data analysis and pattern detection, I utilized the Pan Tompkins algorithm for QRS complex detection and filtering techniques for respiratory rate.

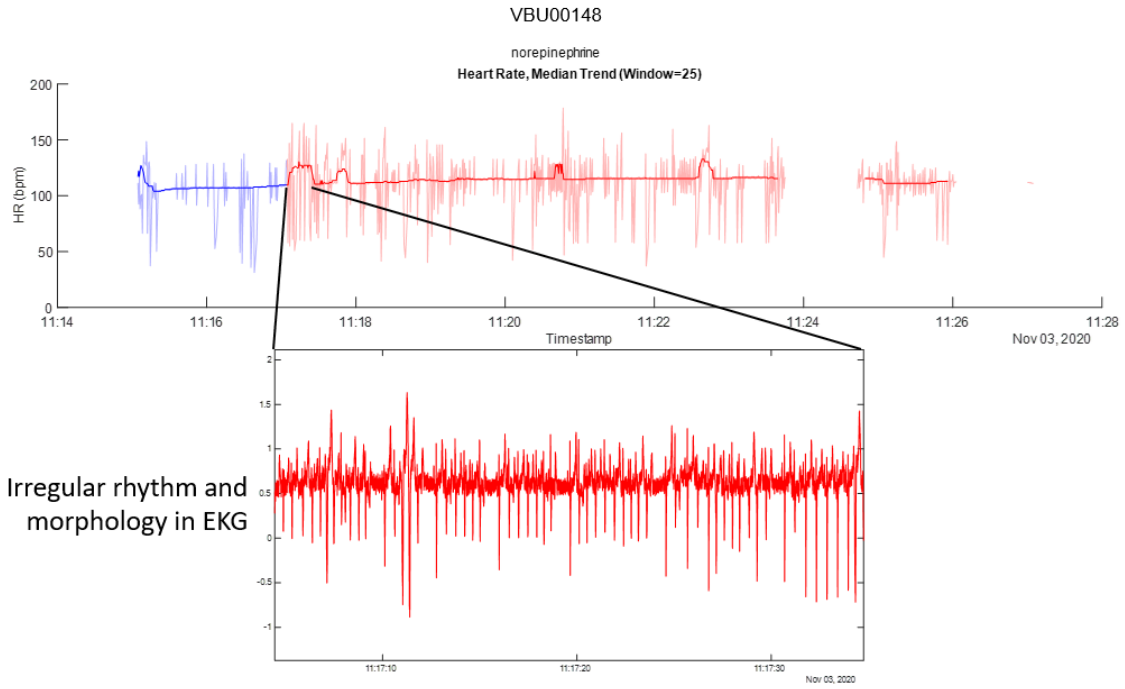

Figure 2-6: Irregular rhythm and morphology in an EKG causes overestimations in heart rate. For animal study VBU00148, continuous heart rate during norepinephrine was calculated using the EKG signal. A moving median was applied to the continuous heart rate signal with a window length of 25 beats.

An external MATLAB script based on the Pan Tompkins algorithm was used to identify heartbeats in a raw EKG signal [21]. This algorithm, developed by Jiapu Pan and Willis J. Tompkins, uses various digital analyses of the slope, amplitude, and width of an EKG signal to identify QRS complexes [22], which correlate to the depolarization of the ventricles and subsequent muscle contraction [4]. The algorithm also incorporates a bandpass filter to reduce noise from EKG signal interferences and increase detection sensitivity, making it a reliable method for detecting heartbeats with over 99% accuracy. I also experimented with layering my own filtering techniques on top of the algorithm, such as applying a moving median across the RR intervals (amount of time between two consecutive QRS complexes) within a segment of data and replacing the times identified as outliers using the `filloutliers` function. However, the final method for estimating heart rate excluded this interpolation of missing beats due to concern regarding inaccurate results.

Solving the issue of respiratory rate variation was more straightforward and merely required the knowledge of the animal's respiratory rate. Respiratory rate was calculated by finding the upper and lower peak envelopes of a section of data and then finding the distance, or number of sample points, between each peak. The `envelope` function was used to find the peak envelopes. The peak-to-peak distances were converted to breaths per minute using the sample rate. When comparing the same section of data in its raw form against its filtered form, there was a noticeable amount of noise eliminated from the signal. A range of respiratory rates for filtering were also tested, from a few breaths per minute below the average rate to a few breaths above. It was found that using the average rate over a small section of data still proved to be the best method for filtering out as much variation as possible.

Another challenge with data analysis was related to variation introduced by the measurement methods used during the animal studies. While the animals are supported by the Impella, changes in the Impella speed noticeably affected certain physiological metrics measured by the reference catheters. Naturally, the measurement of stroke volume fluctuates drastically when Impella support changes. The calculation of stroke volume is reliant on the signal from the pressure-volume (PV) conductance catheter in the left ventricle, which captures both native heart and device flow contributions. When the continuous cardiac output pinging sequence is initiated on the Impella, there is an initial period of calibration to find the best level to perform the pinging sequence, and these speed ramps up and down produced significant changes in the mean stroke volume trend (Figure 2-7). Similar effects with the LVEDP metric and moving heart rate were found. To avoid those effects, any data points that were not measured at a constant Impella speed for a certain amount of time were excluded. Any data sections taken during the pinging rounds were also excluded, as the pinging process alternates the speed between high and low support levels quickly.

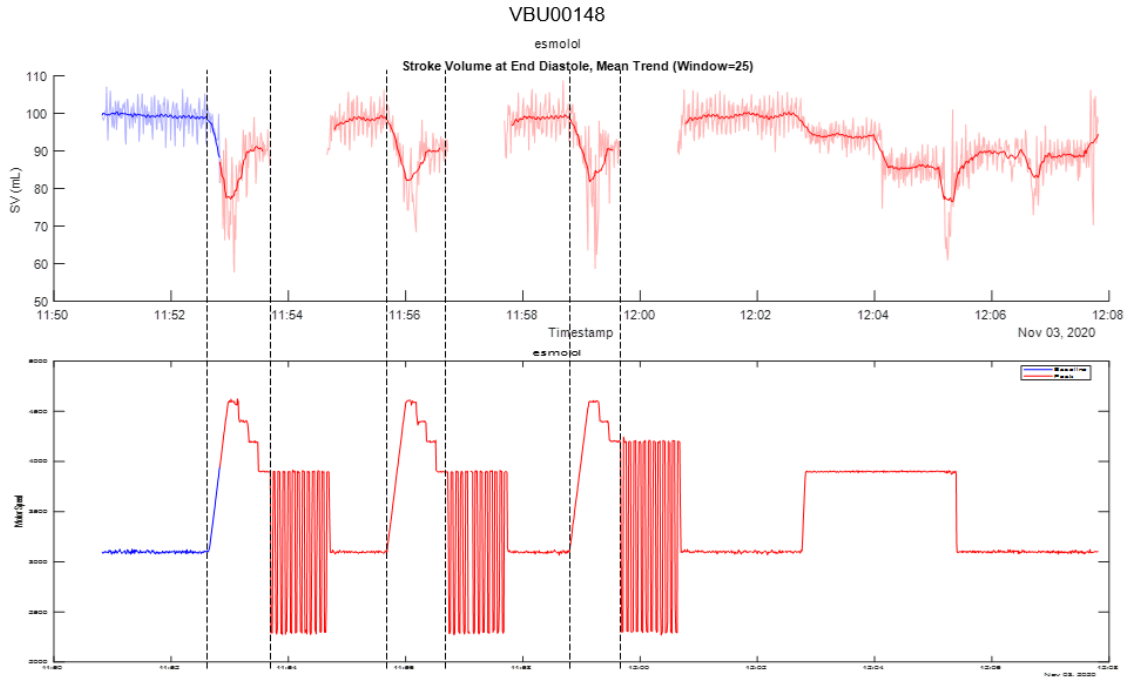

Figure 2-7: Abrupt changes in Impella flow speed produce corresponding fluctuations in observed stroke volume. For animal study VBU00148, continuous stroke volume during esmolol was calculated using the pressure-volume catheter. A moving mean was applied to the continuous stroke volume signal with a window length of 25 beats. The dotted lines mark sections of simultaneous fluctuations in stroke volume and Impella speed signals.

2.1.3 Summary of learnings

Several takeaways regarding the implementation of the trajectory vector approach and the feasibility of the method to detect dynamic state changes were realized. There were multiple challenges associated with differentiating true cardiac events from naturally occurring physiological variation and measurement-related noise. The usage of specialized filtering techniques on raw hemodynamic data are critical to mitigate the influence of variability in animal state identification. The utility of clustering analysis for detecting unknown patterns in cardiac behavior was discovered, motivating future exploration of additional clustering methods for optimal model fitting. Employing z-score standardization across a distribution of data raised the question of whether the changes caused by drug effects are actually independent of baseline state. This topic is key to understanding the potential of the trajectory vector approach as a diagnostic and monitoring tool generalizable to a wide population of patients. Additional techniques somewhat explored in this section, such as the identification of baseline state in an animal and the continuous detection of changes in cardiac state, are pivotal for validating the utility of the trajectory vector method in the clinic. Due to a lack of knowledge of the timing and behavior of cardiac events, these techniques can help inform clinicians of a patient's native physiological baseline and how their cardiac state evolves over time. When equipped with the computational methods developed in this exploration, the trajectory vector approach has clinical value in detecting dynamic trends within the performance-load relationship that even the most experienced clinicians may miss.

2.2 Conducting a set of controlled animal studies

In light of the experience above, the feasibility of the performance-load-based trajectory vector approach was evaluated in a separate set of controlled animal experiments. At minimum, a healthy porcine model was needed to test the feasibility. Swine models are common to use for cardiovascular studies due to having similar anatomic and physiological characteristics to those of humans [23]. However, there left many un-

knowns regarding the studies, such as which pharmacological interventions to use to simulate different physiological states, whether to include an acute cardiogenic shock model, and what type of hemodynamic data to collect.

To observe a range of shifts in the P-L relationship, the selected interventions must have influence over afterload or contractility in either direction. Inducing a wide variety of changes in physiologic state allows comprehensive testing of the trajectory vector's capability to differentiate states. Consequently, the relevant categories of pharmacological agents were narrowed down to: (1) antihypertensives, which lower blood pressure; (2) vasodilators, which dilate the blood vessels; (3) vasoconstrictors, which constrict the blood vessels; and (4) inotropes, which change the force of muscular contractions [24]. The antihypertensive category can be further divided into relevant subcategories: (1) beta-blockers, which reduce heart rate and force of contractions; (2) calcium channel blockers, which interrupt the movement of calcium into cells and thereby decrease contractility; and (3) ACE (angiotensin-converting enzyme) inhibitors, which expand blood vessels by lowering angiotensin II levels. Past animal protocols conducted in our laboratory were referenced for insight into the drugs that were successfully administered.

Several factors were considered when selecting the pharmacological interventions for these studies. The interventions must have the correct intended drug effect. Certain drugs also have both primary and secondary effects related to receptor binding affinity, which enable local physiological effects and innate compensatory mechanisms [24]. Preference was for agents with a dominant primary effect and minimal secondary effects to reduce confounding factors when analyzing drug effect. Due to the time constraints of an eight-hour study, the onset of action, or how much time it takes the drug effect to be prevalent after administration; duration of action, or the length of time the particular drug is effective; and half-life of the drug were also important to consider. I also kept in mind the availability of these interventions and difficulty in storing and administering them through an intravenous (IV) drip. Based on those factors, vasodilator nitroprusside, vasoconstrictor phenylephrine, positive inotrope dobutamine, and beta-blocker esmolol were selected to simulate the variety of states

modeled by the P-L relationship (Figure 2-8).

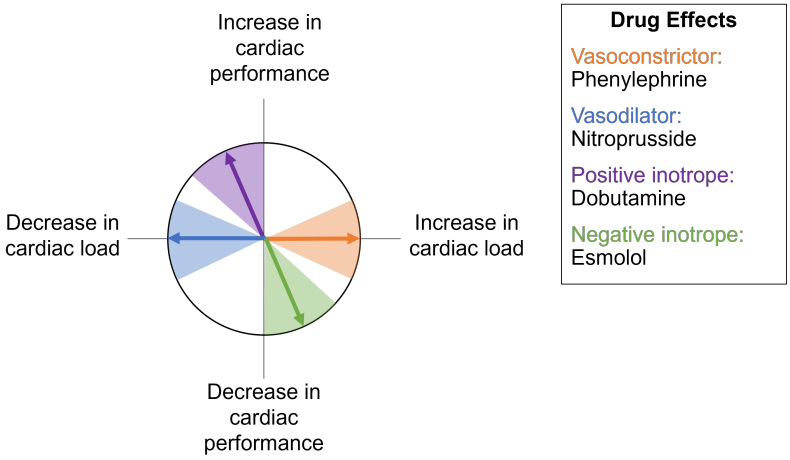

Figure 2-8: Expected shifts in the performance-load relationship produced by inotropic and vasoactive drugs depicted as trajectory vectors. Phenylephrine and nitroprusside affect vascular tone, resulting in changes in afterload. Dobutamine and esmolol affect contractility, resulting in changes in both afterload and cardiac performance.

Completely defining the P-L relationship requires the collection of both LVEDP and CO measurements. A critical aim of this work is to test the feasibility of this trajectory vector method and see whether it can be translated to the clinic in the form of an algorithm on the Impella platform, eliminating the need for extra percutaneous interventions. Therefore, measurements from indwelling catheters (PV catheter in the left ventricle for LVEDP and thermodilution through the pulmonary artery catheter for CO) served as the reference against which to validate measurements from the Impella.

Creating a comprehensive data set to test the capability of the trajectory vector approach requires administering drugs at different doses as well as collecting data at multiple Impella support levels. The method may pick up on these changes in dose response and support level and evaluate how their magnitudes might affect the trajectory response of a given drug. Given the tight time constraints of the study, drugs were administered at just two different doses (low and high) and two different Impella support levels (P-3 and P-6), also referred to as p-levels.

Several questions were posed to be answered by the processes and results from

conducting this series of animal studies. Each question and the corresponding course of action to address it through the animal studies and subsequent data analysis are listed in Table 2.1.

Table 2.1: Questions regarding feasibility and capability of the trajectory approach and their corresponding course of action

Key Question	**Course of Action**
Can progression of a cardiac state be monitored continuously?	Collect dynamic hemodynamic data in a 2D performance-load relationship
Can significant physiological responses be differentiated from local physiological variation and measurement-related noise?	Filter out variation from raw data, apply cluster analysis, and establish trajectory vectors to see if patterns emerge in physiology
Are drug responses independent of baseline state?	Compare metrics of baseline state to trajectory vectors of various drug effects
For a particular physiological state, what does the trajectory look like?	Compare trajectory vectors of a particular drug across all animals
How does the level of Impella support affect the changes in state?	Compare magnitude and angle of trajectory vector to level of Impella support
How does the dose of a drug affect the changes in state?	Compare magnitude and angle of trajectory vector to dose of drug

Chapter 3

Methods and Materials

This chapter details the finalized animal study protocol and computational methods to present performance-load hemodynamic data through the trajectory vector approach.

3.1 Animal study protocol

With the components of the study finalized, three study aims were defined as follows: (1) Optimize methods of data acquisition to evaluate baseline and drug-impacted left ventricular function using reference catheters and the Impella, (2) Obtain data to investigate left ventricular responses to left-sided unloading by the Impella on multiple support levels, and (3) Obtain data to investigate left ventricular responses to vasoactive and inotropic agents using different dosages during left-side unloading by the Impella on multiple support levels.

3.1.1 Protocol equipment and setup

Catheters were used to capture reference hemodynamic measurements. To collect left-sided hemodynamics, a Millar pressure sensor was inserted via the femoral artery, and a Millar PV catheter was inserted via the carotid artery. Right-sided hemodynamic measurements were collected using the Swan-Ganz PA catheter and Millar PV catheter inserted via the jugular vein, as well as the Millar pressure sensor inserted

via the femoral vein. An IVC occlusion balloon was also inserted via the femoral vein. Additional equipment included an external arterial pressure sensor inserted via the femoral artery, an external central venous pressure sensor inserted via the jugular vein, and two sets of EKG leads.

The Impella CP was used as the paradigmatic device to simulate the clinical setting in which a patient with cardiogenic shock may be supported by a percutaneous ventricular assist device. The Impella CP is an intravascular microaxial pump that supports a patient's circulatory system by delivering blood from the left ventricle into the ascending aorta [16]. The device was inserted via the femoral artery and positioned such that the pump inlet rests in the left ventricle and the outlet resides in the ascending aorta, crossing the aortic valve. A controller system allows the user to control Impella flow performance, monitor catheter alarms, and manage real-time catheter position across the aortic valve. Pump flow is controlled by altering the motor's rotational speed based on the pressure difference across the device. Metrics measured and recorded by the device include motor current and motor speed, as well as aortic pressure found through an integrated optical pressure sensor and estimated blood flow rate produced by the pump.

The pump was also used to collect algorithmic hemodynamic measurements for future validation of its utility as a joint support-monitoring device. LVEDP can be derived through a hysteretic relationship between motor current and pressure head [17]. The motor current is a readily available measure of the pump's electrical power and directly related to the load on the pump. The pressure head is the pressure gradient across the pump and varies based on ventricular function during the cardiac cycle (i.e. ventricular filling or ejection). The resulting hysteresis loop created from adjusting motor current to maintain a specific motor speed within unstable pressure conditions allows the identification of LVEDP during a cardiac cycle. An algorithmic-based CO comparable to the clinical standard of thermodilution CO is calculated using a lumped parameter model comprising of both heart and device flow contributions [18]. By quickly fluctuating motor speed in square wave pulses, changes in flow and consequently changes in aortic pressure are generated, facilitating estima-

tions in systemic vascular resistance. Systemic vascular compliance can be derived from known pressure, pump flow, and SVR during diastole. Total cardiac output, a combination of native and pump flow, can then be calculated by inputting the approximated systemic vascular resistance and compliance with measured arterial pressure into the lumped parameter model. The fluctuating square wave motor speed process is hereby referred to as the CO pinging calibration sequence.

3.1.2 Protocol steps

For each animal study (n=4), a controlled protocol with four pharmacological interventions administered at two doses and supported by two p-levels was implemented. The Yorkshire pig served as the healthy animal model. Once the relevant catheters were calibrated and inserted, hemodynamic data was collected before Impella pump insertion. After the Impella pump was inserted, the sequence of data collection during the baseline before each drug was initiated.

The data collection sequence is as follows. First, mean arterial pressure (MAP) and heart rate were recorded. With the support level at P-6, one round of the CO pinging calibration sequence and one thermodilution triplicate was performed to collect both Impella and reference cardiac output data. A 15-second period was then allotted to ensure adequate hemodynamic data collection. Data was also collected during two separate inferior vena cava (IVC) occlusions for analysis of the slope of the end-systolic pressure-volume relationship (ESPVR), a common contractility metric [25]. The occlusions were performed with a breath hold at end expiration to minimize the effect of respiratory variation on the slope calculation. This entire data collection sequence was repeated at the P-3 support level.

During drug administration, a bolus was first given, followed by the initiation of a continuous IV drip at a low dose. The drip rate was adjusted as needed to meet the target hemodynamic metrics. Once the drug reached steady state based on observation of the hemodynamic signals, a set of iStat blood gas measurements, including mixed venous oxygen saturation (SvO2) were taken to ensure adequate perfusion. The aforementioned data collection sequence with pinging, thermodilution, and IVC

occlusions was conducted at both Impella support levels. Once data collection was completed, the IV drip rate was increased to meet the high dose level with adjustments made as needed. After similar data was collected during this section, the drip was discontinued and a period of approximately 5 to 15 minutes was initiated to wash out the drug. The animal weights, drugs, bolus amounts, doses, concentrations, and target thresholds for each study are listed in the tables in Appendix A. During the studies, some additional data was collected for separate projects, such as abdominal aortic pressure and pericardial pressure during a simulated pericardial effusion.

3.1.3 Protocol limitations

Unfortunately, there were several limitations to the series of animal studies. Most significantly, the protocol did not include a cardiogenic shock model due to time constraints. However, analyzing data from an acute disease model is imperative to validate that the trajectory vector method can not only detect changes in relatively healthy states, but can also evaluate changes in a simulated clinical case in which Impella support is needed. In addition, various adjustments were made to each protocol as the series of studies progressed, mainly due to concerns of timing and overstressing the animal. Data at the high dose level for certain drugs were not collected in every study. The studies have a relatively small sample size of 4, so additional studies should be conducted in the future to gather more comprehensive data.

3.2 Analytical methods

Analysis of the data collected during the four animal studies was an extensive process with multiple steps. The following sections describe the steps taken and methods developed to produce the trajectory vector analysis, which were applied for the data set from each animal study.

3.2.1 Data configuration

Since the hemodynamic data from the catheters and the Impella were recorded on separate systems, the signals had to be synchronized properly and combined into a series of files. These files include information such as the timestamp, pressures, and motor speeds, and the data is taken at a sampling rate of 250 Hz. Additional required files include a file with all of the thermodilution triplicate measurements taken through the course of a study and a file containing the instances of drugs and their corresponding doses. Once the relevant files were properly set up, sections of data aligning with the pinging sequences were identified so they could be excluded in later analysis.

3.2.2 Frank-Starling representation of animal states[1]

An overview of the data analysis process for this subsection is depicted in the flowchart shown in Figure 3-1. Data analysis was separated into the evaluation of baseline states prior to each intervention and the evaluation of steady-state drug states. The first step was to get an accurate metric of left ventricular volume. In this set of studies, a pressure-volume (PV) catheter was used to measure continuous volume in the left ventricle. The catheter uses electrodes along its end to measure changes in conductivity which correspond to changes in volume, outputting a raw voltage signal. Since the placement of the left ventricular PV catheter and correlating volume signal often fluctuate due to changes in flow and muscle contraction inside the ventricle, the raw voltage signal corresponding to left ventricular volume was calibrated at every animal state and p-level (e.g. Baseline Nitroprusside at P-6, High Dose Dobutamine at P-3). In addition, the catheter measures real-time flow within the ventricle, which includes both native and Impella contributions. To get an accurate measurement of stroke volume, which is only during systole, flow from the Impella pump during diastole must be excluded.

[1] Although the eventual context surrounding the trajectory vector approach is based on a broad performance-load relationship, in this work we still rely on the analysis of metrics of LVEDP and CO that traditionally outline the Frank-Starling curve.

Volume Calibration

The volume calibration sequence, which also includes a conversion of voltage to volume units, is as follows. If present, large sections of noisy data and sections aligning with the pinging CO sequence were excluded from the raw volume signal. Next, for the given animal state, the section of volume signal aligning with the corresponding thermodilution period was isolated. Cardiac output was averaged over the thermodilution triplicate measured during the state. Average heart rate during the thermodilution period was also calculated by identifying the QRS complexes. Several filtering techniques were applied to reduce error and minimize outlier effects in the heart rate calculation, such as validating the QRS complex locations with points on the left ventricular pressure tracing corresponding to end diastole and excluding any noisy beats corresponding to arrhythmias or premature ventricular contractions (PVCs). With both the average cardiac output and heart rate, average stroke volume during the thermodilution period could be estimated using the equation $CO = HR * SV$ [4].

Within the thermodilution section of the signal, only subsections of data that were collected at constant Impella motor speed corresponding to the intended support level were included. In every subsection of constant motor speed, the stroke volume represented by voltage and the volume ejected by the pump during diastole were calculated for every beat. For every peak identified in the volume signal, which represents one beat, the voltage change and Impella flow across the beat were used to find the Impella's diastolic volume contribution. Outliers among the stroke volume voltage values and diastolic pump volume values were removed. Using the average pump volume per beat during diastole subtracted from the average stroke volume during thermodilution, a scaling factor was applied to the entire raw volume signal to get continuous left ventricular volume in liters. The scaling factor can be described in the following equation, where SF is the scaling factor, SV_{volume} is the average stroke volume during the thermodilution period in liters, PDV is the average pump diastolic volume during the thermodilution period in liters, and $SV_{voltage}$ is the average stroke volume during the thermodilution period in voltage:

$$SF = (SV_{volume} - PDV)/SV_{voltage} \tag{3.1}$$

Extracting LVEDP and CO

Following left ventricular volume calibration, the desired section of data for the given animal state was identified, spanning from two minutes before the start of the thermodilution period to the end of the period. For every constant motor speed subsection within the section of data, all instances of LVEDP were identified in the left ventricular pressure signal from the PV catheter. The timing of end diastole can be approximated by identifying the QRS complex in an EKG signal [26]. Additionally, stroke volume was calculated for every identified beat within a subsection using the equation $SV = EDV - ESV$, where EDV and ESV are end-diastolic and end-systolic volume respectively [4]. End-systolic and end-diastolic volume were found by identifying the trough and peak of a beat within the calibrated volume signal. After outliers were removed, the SV data points were converted into CO using average HR, found through QRS complex identification. In order to conduct a beat-to-beat Frank-Starling analysis, only the instances of LVEDP and CO belonging to the same cardiac cycle were included. Lastly, respiratory variation was filtered out by applying a moving average to the remaining data points, with a window length equivalent to the number of heartbeats per breath. The average respiratory rate during the data section, upon which the window length is based, was calculated using envelope detection of the aortic pressure signal and the location of peaks and troughs among the upper and lower envelopes.

All outliers were removed using the default version of the `rmoutliers` function.

3.2.3 Cluster analysis

As mentioned previously, the DBSCAN method was implemented as an initial attempt at performing cluster analysis. However, there were a multitude of clustering methods with relevance to the collected data sets which were not yet explored. The implementation of two clustering methods, DBSCAN and GMM clustering, are ex-

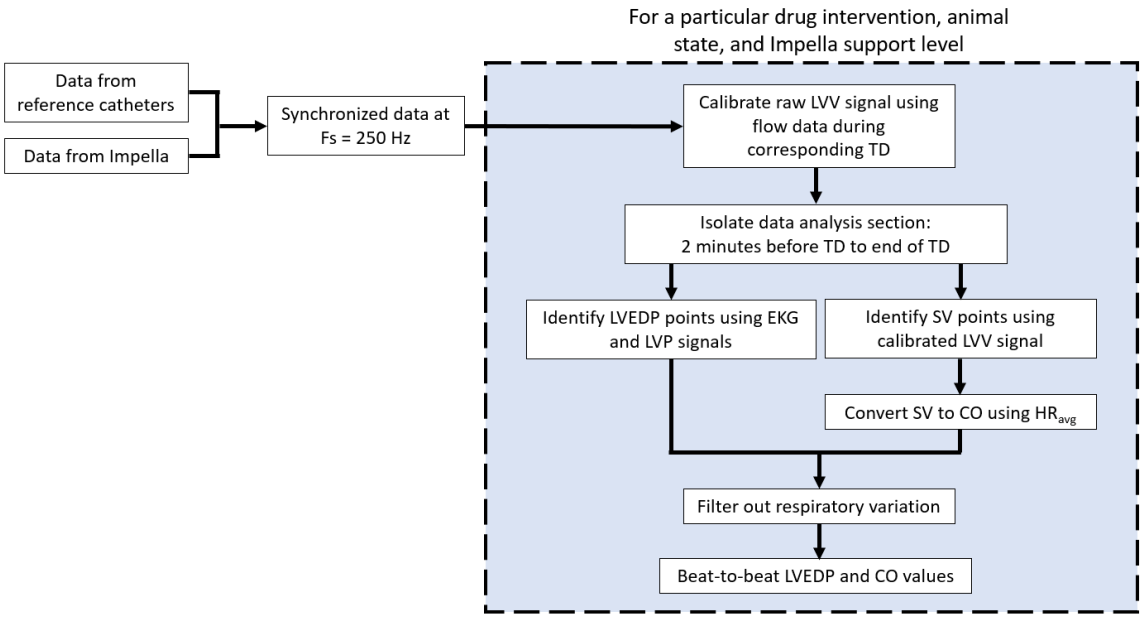

Figure 3-1: Flowchart with an overview of the Frank-Starling beat-to-beat analysis process. After the data is properly configured, a series of steps to extract beat-to-beat LVEDP and CO values is conducted for a particular drug intervention (e.g. dobutamine), animal state (e.g. baseline), and Impella support level (e.g. P-6). LVV=left ventricular volume, TD=thermodilution, LVP=left ventricular pressure.

plained in the following sections. GMM clustering was eventually pursued as the finalized method for cluster analysis as it was more appropriately suited to identify patterns in the highly variable animal data sets and produced results that were more similar to the original groupings of data.

Density-Based Spatial Clustering of Applications with Noise (DBSCAN)

DBSCAN is advantageous for data sets with potential outliers and noise interference, especially because it relies on detecting regions with high density. It also does not restrict the identified clusters to particular shapes or sizes, and does not require prior knowledge of the number of clusters present within the data. It was found to be beneficial for this animal data due to the variability across the hemodynamic metrics and natural grouping seen between the physiological states. The basis of my DBSCAN implementation is the `dbscan` function, which groups data points into clusters using the DBSCAN algorithm developed by Ester et al [19]. The function takes in

the data matrix[2], the neighborhood range parameter ϵ (representing cluster radius), and the minimum number of points for a cluster *minpts* (representing the density threshold) to determine clustering assignments.

For a given data set, ϵ was chosen based on a sorted k-distance graph, a common heuristic method [19]. The graph displays the k-nearest-neighbor Euclidean distances, where k is set to *minpts*, for each point in ascending order. The elbow of the graph, or the point in which the slope of the plot significantly changes, represents the threshold of the smallest cluster possible (Figure 3-2).

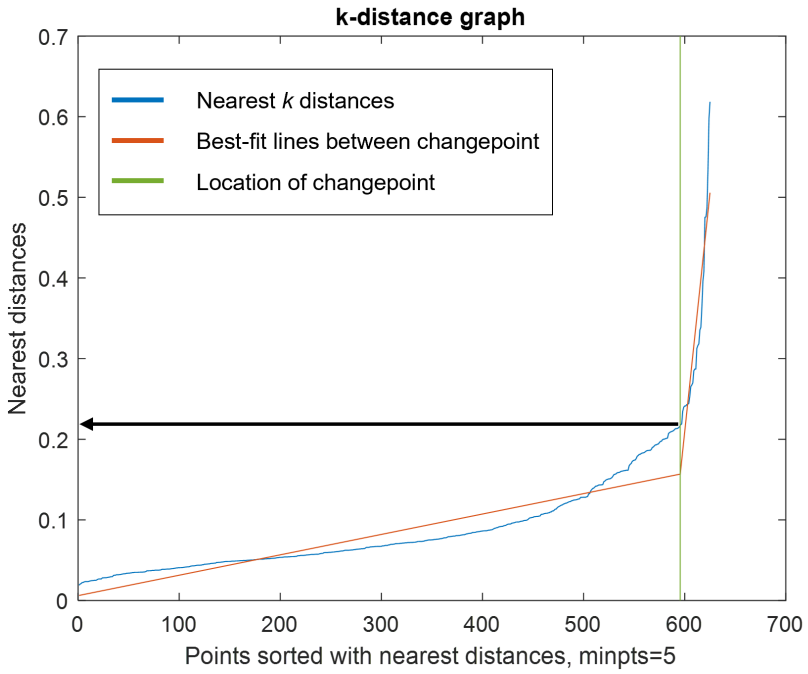

Figure 3-2: k-distance graph for evaluating ϵ at a given *minpts* for DBSCAN implementation. The graph displays the k-nearest-neighbor Euclidean distances, where k is set to *minpts*, for each point in ascending order. In this case, $minpts = 5$. The elbow of the graph, or the point in which the slope of the plot significantly changes, represents the threshold of the smallest cluster possible. ϵ is set as this threshold. Best-fit lines were fitted to the plotted curve to find the changepoint, representing the elbow of the graph.

Defining the parameter *minpts* is generally more straightforward, with common default values such as four for two-dimensional data or twice the number of data

[2]When applying a clustering method, the data must be structured as an N x P matrix, with the first dimension representing the number of data points in the study N and the second dimension representing the number of variables P (in this case, P=2 for LVEDP and CO).

dimensions [19][27][28]. While fitting DBSCAN clustering models to the data sets, I experimented with a range of *minpts* values (5, 10, 15) and ϵ values (ϵ-.2 to ϵ+.1 in increments of 0.1). Clustering model validation and evaluation of the selected parameters were conducted graphically using silhouette plots, which show a measure of how close each data point in one cluster is to points in neighboring clusters (Figure 3-3) [29].

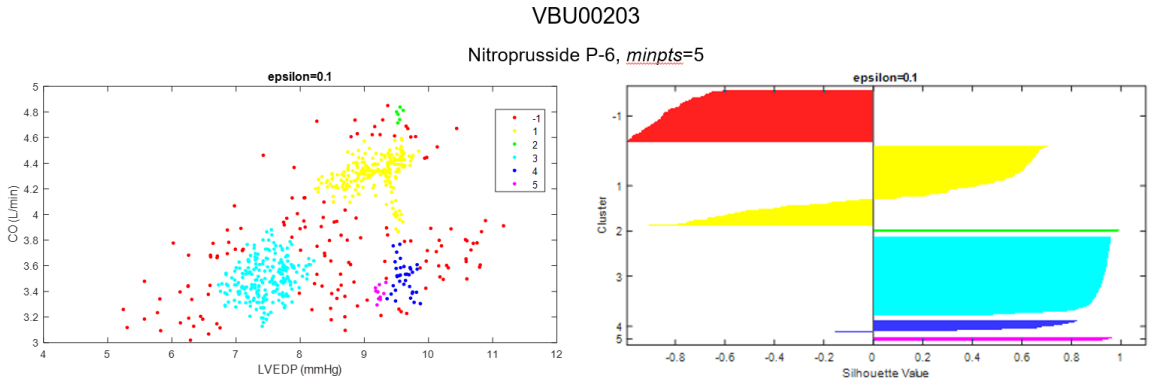

Figure 3-3: Silhouette plot to evaluate clusters assigned by DBSCAN given particular parameters. For the animal study VBU00203, DBSCAN was applied for the baseline, low dose, and high dose states during the nitroprusside intervention at P-6. $epsilon = 0.1$ and $minpts = 5$. Five distinct clusters were identified, along with outliers (assigned to -1). A silhouette plot displays cluster assignments against silhoutte values. A silhouette value is a measure how similar a point is to other points in the same cluster compared to points in other clusters. Higher silhouette values indicate better clustering, while lower or negative values indicate the clustering solution has an inappropriate number of clusters.

Gaussian Mixture Model (GMM) Clustering

The second clustering method applied to the animal data sets was based upon the Gaussian mixture model (GMM). GMMs are used to represent different normally distributed subpopulations, or clusters, within an overall population [30]. Each cluster is defined by its own covariance matrix, providing a measure of the variance of each individual variable and of the joint variability of each pair of variables [31]. GMM clustering is favorable because it can accommodate clusters with different sizes and correlation structures, and can even partition cluster observations and outliers. Given the variability of the Frank-Starling metrics between baseline, low-dose, and high-

dose states, a Gaussian mixture model fitted to the animal data seemed appropriate. My implementation of GMM clustering utilized the `fitgmdist` function, which fits a Gaussian mixture distribution model of a particular number of components (i.e. clusters) to the data. The function requires the data matrix[2] and the number of clusters k as parameters. In addition, parameters regarding the covariance matrices can be specified, including the type of covariance matrix (i.e. full vs. diagonal) which influences the orientation of a cluster and the relation between the covariance matrices (i.e. shared vs. unshared) which influences the size of a cluster (Figure 3-4).

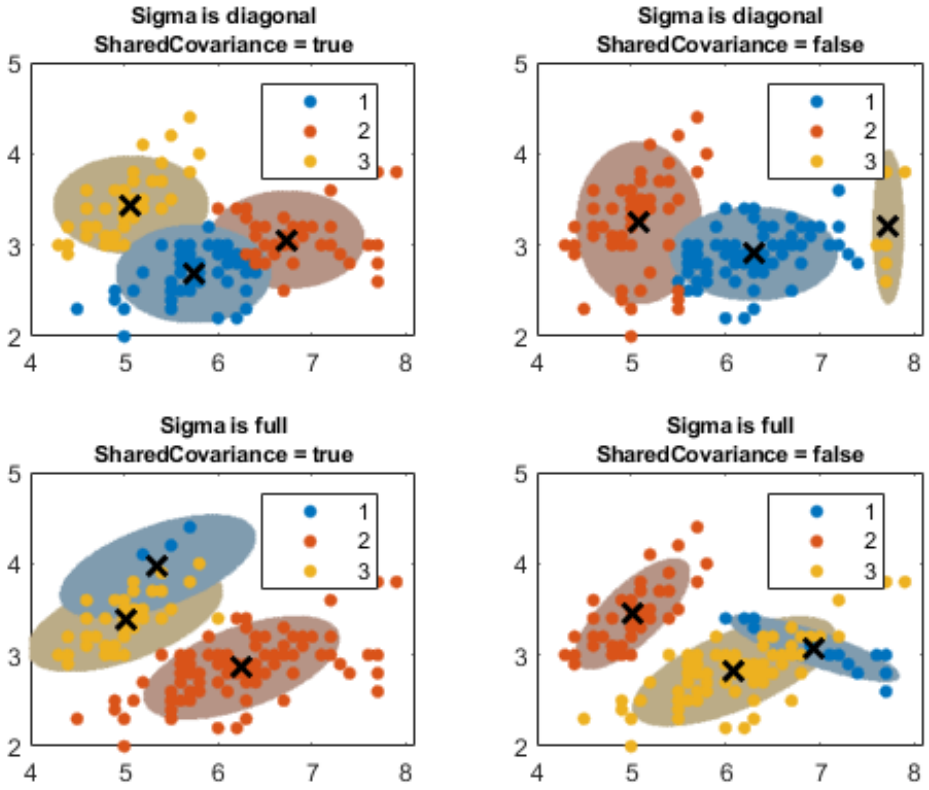

Figure 3-4: Available combinations of covariance structure options for Gaussian mixture model clustering. Σ, representing covariance matrix type, can be full or diagonal. Diagonal matrices indicate that the variables are uncorrelated, forcing the clusters to be directionally aligned with the x and y axes. SharedCovariance, representing the relation between the covariance matrices, can be true or false. Shared covariance matrices indicate that the covariance matrices of all the components are identical, forcing the clusters to have the same size and orientation. Figure from "Cluster Using Gaussian Mixture Model" MathWorks documentation [32]

When applying this method, each data point is assigned a posterior probability, a measure of association strength, of belonging to each cluster. This enables two clustering options: (1) hard clustering, in which each data point is assigned to exactly one cluster based on maximizing the cluster's posterior probability; and (2) soft clustering, in which each data point can be assigned to more than one cluster based on its posterior probability to each cluster. I decided to pursue the soft clustering option to provide more flexibility in my analysis and possibly exclude points that are not statistically significant enough to be differentiated from certain physiological events.

Establishing the soft clustering method for a desired number of clusters and a predefined covariance structure was the first step in creating a functional GMM clustering implementation. A GMM model was fitted to the data for a particular drug and p-level, with k=3 based on the number of animal states (i.e. baseline, low-dose, high-dose). MATLAB's default covariance structure, a full unshared covariance matrix, was used. A regularization parameter value was set to a small positive scalar (i.e. 0.1), which is added to the diagonal of every covariance matrix to ensure that the estimated covariance matrices are positive definite. After model fitting, the posterior probability of each Gaussian mixture component in the model was calculated. For every cluster, the points with posterior probabilities that fell within a specific threshold range were identified as those belonging to multiple clusters, which I defined as "overlapping points." The threshold range was set as 0.4 to 0.6, covering the middle 20% of the posterior probability range. Clustering assignments with the overlapping points identified were plotted in a Frank-Starling representation and compared to the original groupings of data (Figure 3-5).

While specifying the number of components and covariance structure for a GMM model simplified implementation and allowed a rapid trial and error process, using predefined parameters is insufficient for achieving the optimal model fit. In many real-life applications, the appropriate number of components k and covariance structure Σ are unknown. I expanded upon my initial soft clustering technique by testing a range of k values (i.e. 1 to k+2) and all combinations of covariance structure for tuning GMM model fitting. The initial k value selected for the basis of the range

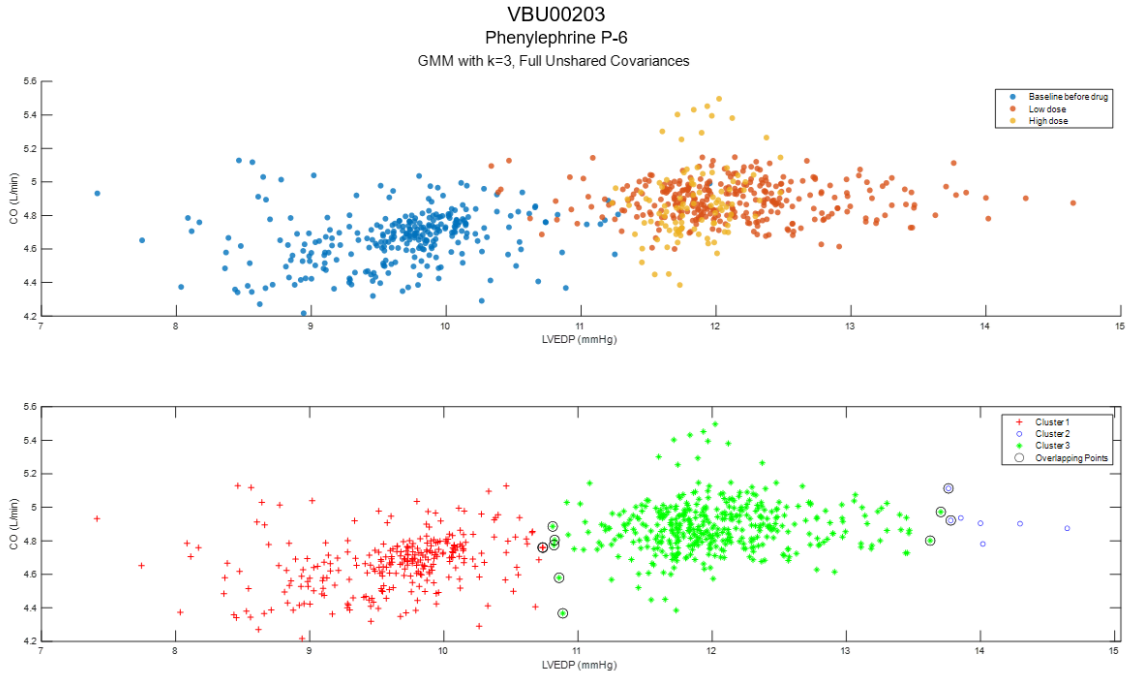

Figure 3-5: Gaussian mixture model with default parameters fitted to animal data. For the animal study VBU00203, GMM clustering was applied to the data during phenylephrine at P-6. Default parameters include $k = 3$ and full unshared covariance matrices. Resulting cluster assignments in the bottom subplot were compared to original state assignments in the top subplot. Points identified as belonging to multiple clusters, using the threshold [0.4-0.6], are circled in the bottom subplot.

was chosen either as k=2 or k=3, depending on the data of the particular animal study. Additional options were standardized across all the models. The regularization parameter value was set to 0.01, decreasing it from the previous value to reduce error generated in the model, and the maximum number of iterations to reach model optimization was set to 10,000, using a large number to reduce the chances of convergence to a local optimum. The total number of models generated for one data set is related to the number of parameters tested:

$$nModels = nK * nSigma * nSC \tag{3.2}$$

where $nModels$ is the number of Gaussian mixture models generated for the data set, nK is the number of k values, $nSigma$ is the number of covariance types, and nSC is the number of shared covariance parameter options.

Two popular information criteria, the Akaike information criterion (AIC) [33] and the Bayesian information criterion (BIC) [34], were used to evaluate the various GMMs fitted to the data and to guide model selection. These information criteria are based on the maximum likelihood method, which estimates the parameters for a statistical model such that they maximize the likelihood that the model produced the observed data [35]. Both AIC and BIC reward goodness of fit and penalize overfitting; smaller values correspond to better-fitting models. However, AIC tends to choose models that overfit due to its linearly increasing penalty term, while BIC can select underfitted models as the number of data observations increases due to its asymptotically inefficient penalty term [36][37][38]. To balance the effects of the two penalty terms, I found the average of AIC and BIC for every model and used the minimum average value to select the optimal model for the data set during the particular pharmacological intervention and p-level.

Soft clustering with the same threshold range was performed on the optimal model. Final clustering assignments and the identification of overlapping points were plotted in a Frank-Starling representation and compared to the original groupings of data (Figure 3-6). It can be noted that in this work, clustering was only applied on fixed periods of data for ease and simplification of its implementation. The true value of employing cluster analysis on animal data lies in its capability to capture changing trends over time. In the future, the implementation of clustering in a more continuous fashion, with consideration to the temporal aspect of dynamic cardiac state, should be explored.

3.2.4 Vector analysis

Once the optimally fitted Gaussian mixture models for each data set were selected, the model features were utilized to fit confidence ellipses onto the identified clusters and standardize the data for trajectory vector analysis. First, the original groupings of the data (i.e. baseline, low dose, and high dose), were plotted, with the overlapping points from the model visually identified (Figure 3-7a). Before fitting a confidence ellipse to each cluster, the overlapping points were excluded from the data set to

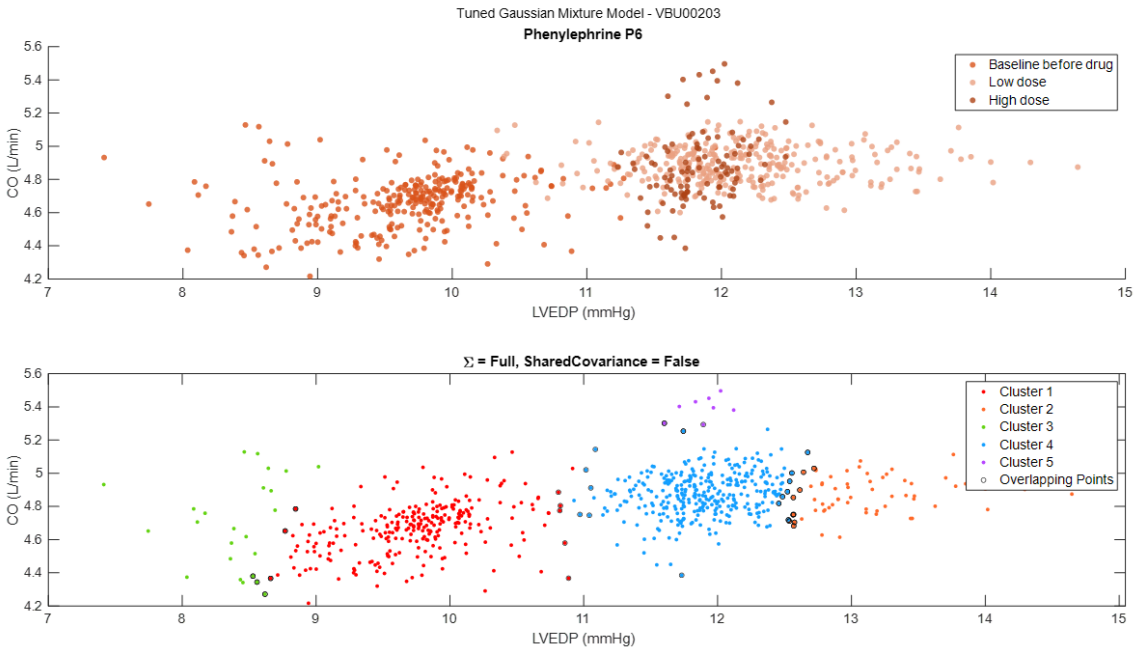

Figure 3-6: Gaussian mixture model with tuned parameters fitted to animal data. For the animal study VBU00203, GMM clustering was applied to the data during phenylephrine at P-6. The optimal parameters, tuned using information criteria, include $k = 5$ and full unshared covariance matrices. Resulting cluster assignments in the bottom subplot were compared to original state assignments in the top subplot. Points identified as belonging to multiple clusters, using the threshold [0.4-0.6], are circled in the bottom subplot.

better distinguish between each model component.

Fitting Confidence Ellipses

The following steps were taken to fit a confidence ellipse for a given cluster. For an ellipse aligned with the x and y axes (i.e. a diagonal covariance matrix), centered at the origin, and with semi-major axis and semi-minor axis of lengths a and b respectively, the general equation is:

$$\frac{x^2}{a} + \frac{y^2}{b} = 1 \tag{3.3}$$

When defining an ellipse for a cluster of data points with a covariance matrix, the size of the ellipse is directly correlated to the spread of the cluster, represented by the eigenvalues of the covariance matrix. The eigenvectors of the covariance matrix corre-

spond to the directionality of the major and minor axes, influencing the orientation, or angle, of the ellipse. Fitting an ellipse at a specific confidence level defines the scale of the ellipse; the scale is based on the critical value in the chi-square distribution at that confidence interval. The resulting equations defining a confidence ellipse fitted to a cluster of points with a full covariance matrix are:

$$(\frac{x-\mu_x}{\sqrt{\lambda_1}})^2 + (\frac{y-\mu_y}{\sqrt{\lambda_2}})^2 = s \tag{3.4}$$

$$\alpha = arctan\frac{\mathbf{v_1}(y)}{\mathbf{v_1}(x)} \tag{3.5}$$

where λ_1 is the larger eigenvalue, λ_2 is the smaller eigenvalue, s is the chi-square critical value at the desired confidence level, α is the angle of the ellipse between the positive x-axis and the major axis, and $\mathbf{v_1}$ is the eigenvector corresponding to the larger eigenvalue [39][40].

Ellipses were fitted at 95% confidence (Figure 3-7b). The `chi2inv` function was used to calculate the inverse cumulative distribution function of the chi-square distribution with df=2 for the Frank-Starling variables, evaluated at p=0.95. The `eig` function was used to determine the eigenvectors and eigenvalues of the cluster's covariance matrix. The ellipses were fit at the correct orientation by applying a rotation matrix using angle α.

Selection of Clusters to Represent Animal States

In some instances, the optimal Gaussian mixture model for the data set identified more clusters than the original three states of baseline, low dose, and high dose. The following outlines the steps regarding the assignment of clusters to represent each animal state, which was primarily based on cluster size and composition.

Every cluster in the model was chosen to represent one of these three states using a threshold criterion. The threshold for the minimum number of points of an animal state needed in a cluster for the cluster to represent the state is defined as:

$$threshold = n(1-(\eta/100)w) \tag{3.6}$$

where n is the number of points in the cluster and w is a weighting factor. The weighting factor ranged from 2 to 2.75 depending on the number of data points in the study. η is a key value influencing the fractional component that scales the threshold. It is defined as

$$df^{\eta} = n \tag{3.7}$$

where df is the degrees of freedom of the data set. Since a cluster with fewer points has less information and more uncertainty regarding the states it can represent, the standard at which a cluster is considered as a valid representative should be higher for smaller ones. Therefore, at a certain dimensionality, η decreases as n decreases, resulting in a larger fraction of the number of cluster points to be set as the threshold.

In addition to meeting the threshold criterion, the cluster also has to have a minimum size equivalent to two times the dimensionality of the data. If both of these criteria are met, the cluster is assigned to the most frequently occurring animal state among its points. Otherwise, the cluster is not assigned to any animal state. As a result, some states were not represented in a Gaussian mixture model. Furthermore, if a cluster has a mix of both low-dose and high-dose points, the low and high dose effects cannot be differentiated, indicating that the cluster can represent both states.

Since there may have been animal states represented by more than one cluster, the animal state assignments were filtered so each state had at most one cluster representation. Among the representing clusters selected in the previous step, the cluster with the most points from that animal state was ultimately selected to represent the state. Unselected clusters were excluded from further analysis. An example of the selection of clustering assignments is shown in Table 3.1 and Figure 3-7.

Standardization of Data and Characterization of Clusters

Using z-scores is a common method for standardizing across a distribution, allowing one to see the probability of a data point occurring in the distribution. It is favorable to use in situations where the units of the variables involved are different, since they can be standardized to a singular unit. In the case of this animal

Cluster number	*n*	Most frequently occurring animal state	Frequency of state	Threshold	Met threshold?
1	81	High dose	80	66.9	Yes
2	21	Baseline	21	18.5	Yes
3	86	High Dose	86	70.8	Yes
4	186	Baseline	186	147.4	Yes
5	198	Low Dose	191	156.5	Yes

Table 3.1: Example displaying the selection of GMM clusters to represent animal states. For the animal study VBU00221, clusters using a GMM were identified during nitroprusside at P-3 (Figure 3-6b). Within every cluster, the frequency of points for the most frequently occurring animal state must meet the threshold to be assigned that animal state. Threshold is calculated using equations 3.6 and 3.7. However, an animal state can only be represented by at most one cluster; the cluster with the most points of that animal state is selected as its representative. Ultimately, clusters 3, 4, and 5 were assigned to the high dose, baseline, and low dose states respectively.

data analysis, the baseline state is treated as the distribution that all other states are standardized to, enabling us to observe the probability of certain physiological events occurring given that baseline distribution. To employ z-score standardization, the data must satisfy two criteria: (1) the entire data set must not be normally distributed so it can be standardized to a specific normal distribution; and (2) the baseline to which the data is being standardized must be normally distributed. The second criterion was already satisfied due to the nature of the fitted model; we can assume each cluster identified by the Gaussian mixture model, including the baseline cluster, can be modeled by a normal distribution with certain variances and covariance. For the first criterion, a Lilliefors test was used to test the null hypothesis that the data during a particular drug intervention and p-level comes from a normally distributed population. If the p-value calculated for the distribution along an individual variable falls below the 5% significance level, the null hypothesis is rejected.

If both variables in the data set, LVEDP and CO, pass the Lilliefors test, the data can be standardized to the normally distributed baseline cluster using the following equation:

$$Z = \frac{x - \mu_{baseline}}{\sigma_{baseline}} \tag{3.8}$$

where Z is the standard score equivalent to number of standard deviations, x is an observed value, $\mu_{baseline}$ is the mean of the baseline values, and $\sigma_{baseline}$ is the standard deviation of the baseline values. New confidence ellipses were fit to the remaining standardized clusters (Figure 3-7c). Cluster characteristics such as the centroid, eigenvalues, eigenvectors, angle, and spread along the x and y axes were recorded.

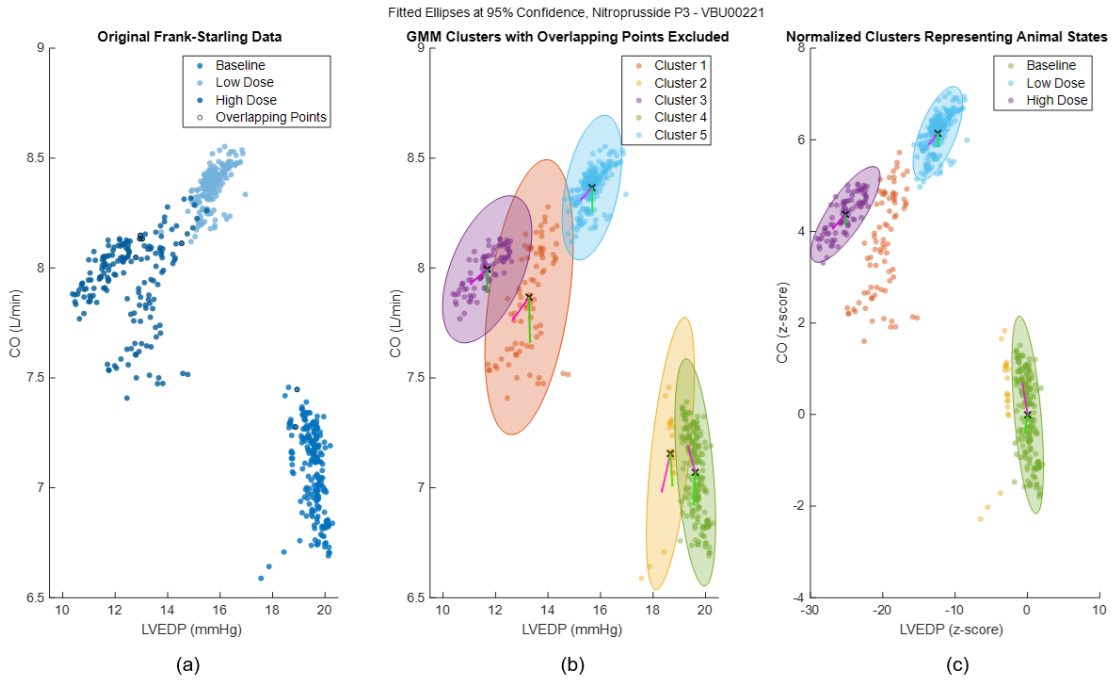

Figure 3-7: Generating normalized clusters based on a fitted Gaussian mixture model to represent animal states. For the animal study VBU00221, a tuned GMM was fitted to data during nitroprusside at P-3. (a) Original groupings of baseline, low dose, and high dose data with identified overlapping points from the fitted model. Overlapping points are excluded in the ellipse fitting. (b) Ellipses fitted on the clusters at 95% confidence. The centroid and eigenvectors, corresponding to the major and minor axes, of each ellipse are marked. (c) Final clusters selected to represent the baseline, low dose, and high dose states. Data is normalized via z-score to the baseline cluster.

Trajectory Vector Representation

Establishing the trajectory vector representation involved analyzing the previously

recorded cluster characteristics of the study's data set. First, the pairwise Euclidean distance was found between the centroids of the baseline cluster and low dose cluster as the length of the unit vector. The end point of the unit vector was calculated by subtracting the x and y values of the low dose centroid from the x and y values of the baseline centroid and normalizing the coordinates to the length of the vector. The origin served as the vector's starting point. All of these analysis techniques were performed during each pharmacological intervention and at each Impella support level. Additionally, the process was repeated for evaluating the effect of the high dose state in relation to the baseline state. The set of vectors were plotted on a unit circle, with their lengths scaled to the largest vector magnitude of the study (Figure 3-8).

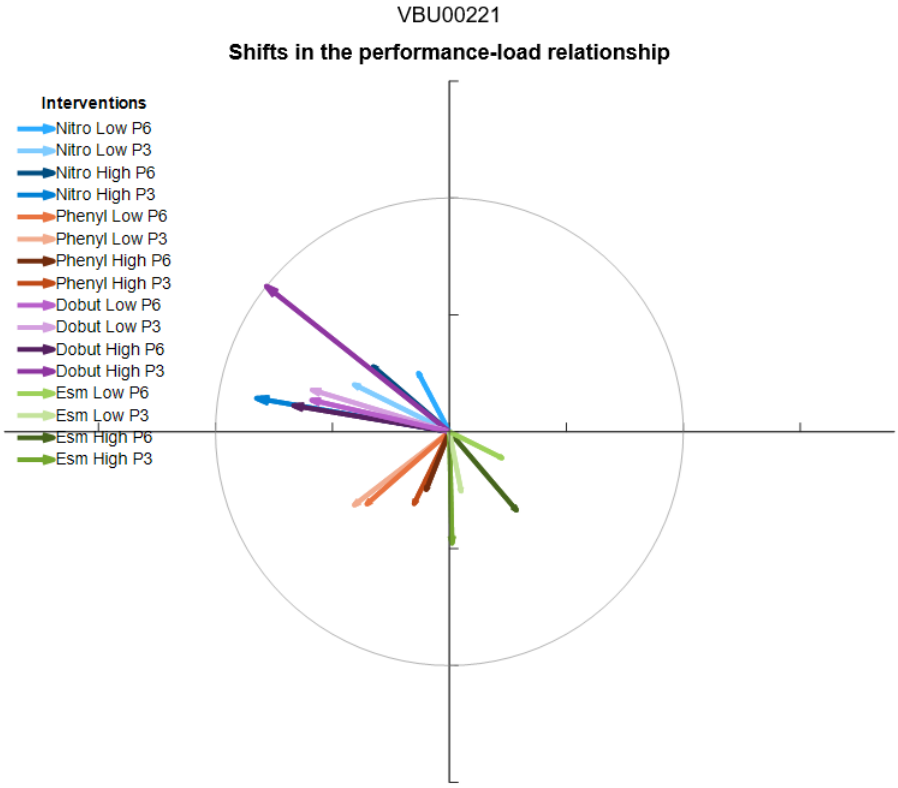

Figure 3-8: Trajectory vectors representing changes from baseline state due to drug effect. For the animal study VBU00221, trajectory vectors were established between the baseline state and low dose state, as well as the baseline state and high dose state, for each intervention and p-level. The ellipses were fitted to the GMM clusters at 95% confidence. Each vector on the unit circle represents a directional shift in the performance-load relationship. Vector lengths were scaled to the largest vector magnitude of the study.

Chapter 4

Results

For all trajectory vector plots, the vectors are defined between the centroids of 95% confidence ellipses, which are fitted to clusters identified by an optimized Gaussian Mixture model for each study. The vectors are displayed on a unit circle, with their lengths scaled to the drug effect with the largest magnitude in the study. Not all animal studies include every intervention state. For particular interventions, the low and high dose effects could not be differentiated with GMM clustering (i.e. VBU00203 Nitroprusside P-3, VBU00203 Phenylephrine P-6, VBU00205 Phenylephrine P-3), producing trajectory vectors of the same direction and magnitude.

4.0.1 Trajectory vectors categorized by study

The trajectory vectors categorized by animal study are shown in Figure 4-1. Dividing the vectors by study allows us to see the variation of responses to the same drugs within the context of a distinct native physiology. The trajectories depict changes from the baseline to low dose and baseline to high dose states at the P-6 and P-3 Impella support levels. Changes in drug effects are referenced to baseline state so we can observe the effect of drug dose on vector magnitude, portrayed by vector length in the unit circle. This relationship can be especially valuable in settings where the first dose of a medication must be titrated at the right amount but drug response is patient-specific. The corresponding vector magnitude can help inform the appropriate

initial drug dose for the patient.

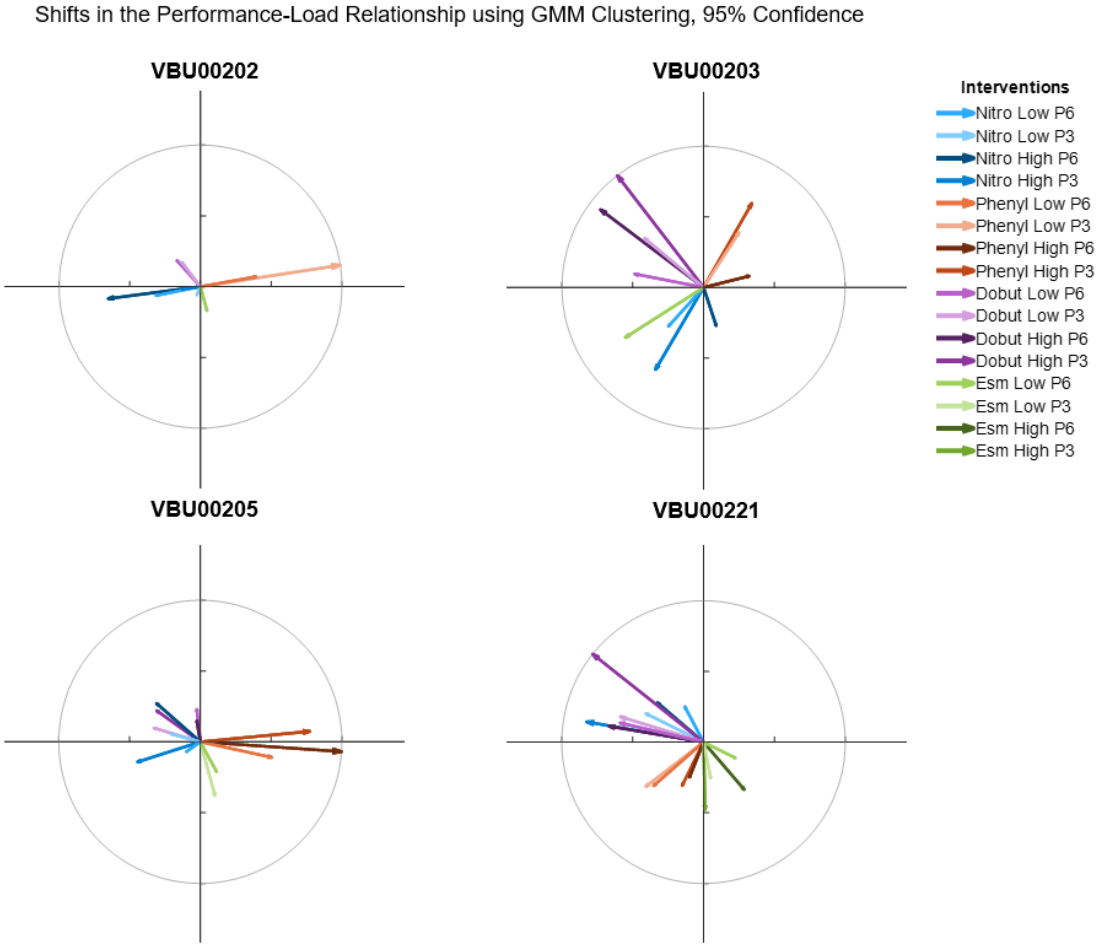

Figure 4-1: Trajectory vectors across four animal studies. The trajectories depict changes from the baseline to low dose and baseline to high dose states for every drug intervention at the P-6 and P-3 Impella support levels.

Changes relative to prior state were also observed. Figure 4-2 shows the trajectories for relative dose responses, in which a low dose state is referenced to the prior baseline and a high dose state is referenced to the prior low dose state. Relative dose response is applicable in situations where the current dose given to a patient needs to be adjusted to achieve a target condition. These vectors that reflect stepped dose titrations can support clinicians' understanding of incremental responses of a patient to a specific medication.

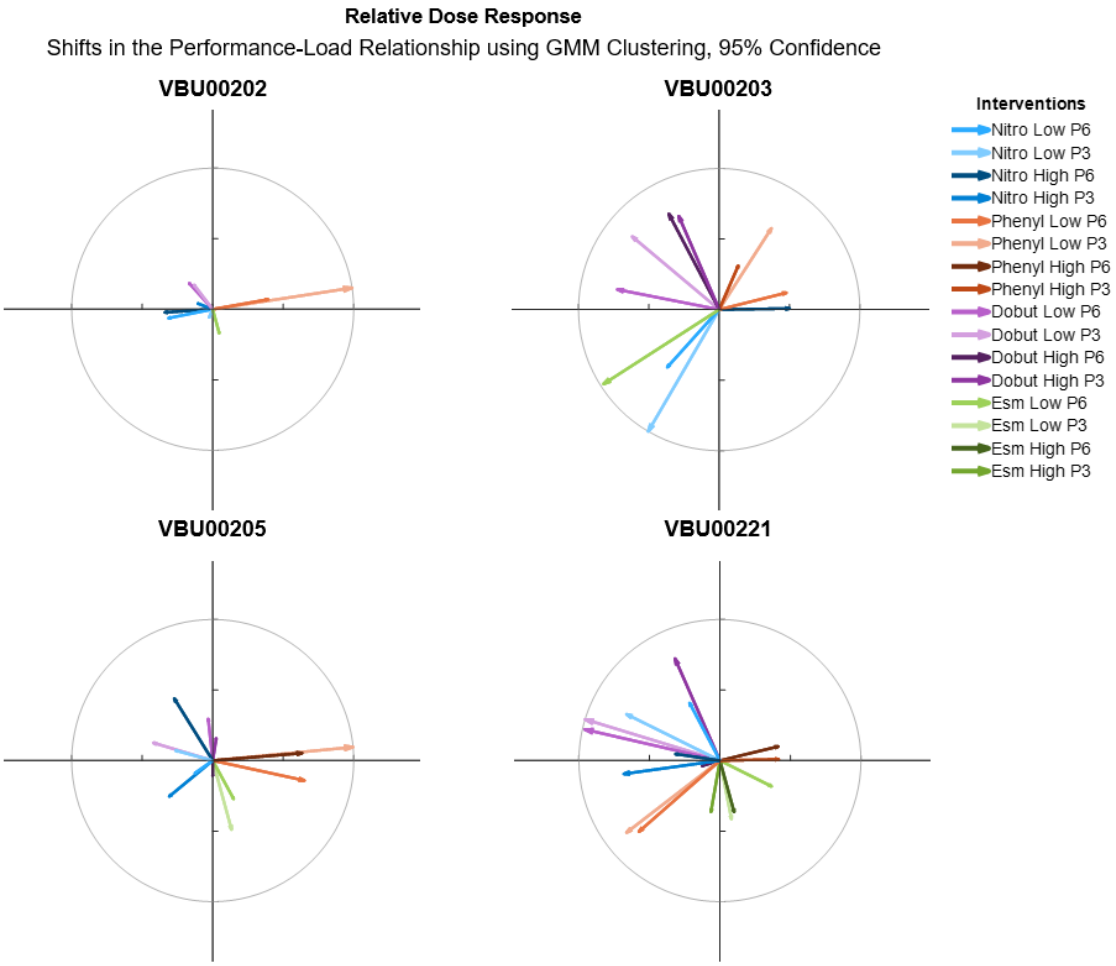

Figure 4-2: Relative dose response trajectory vectors across four animal studies. The trajectories depict changes from the baseline to low dose and low dose to high dose states for every drug intervention at the P-6 and P-3 Impella support levels.

4.0.2 Trajectory vectors categorized by pharmacological intervention and level of Impella support

Trajectory vectors across all four studies were also categorized by pharmacological intervention. Sorting vectors by drug can isolate any repeated patterns in a specific drug response. We can also observe the amount of variation present in said response over the sample population. Further separation by p-level enables evaluation of the influence of Impella support on drug effect, delineated by vector direction and magnitude. Through this analysis, we may be able to see how introducing a device transforms observed physiological response. Figures 4-3 and 4-4 display the vectors organized by

intervention and p-level.

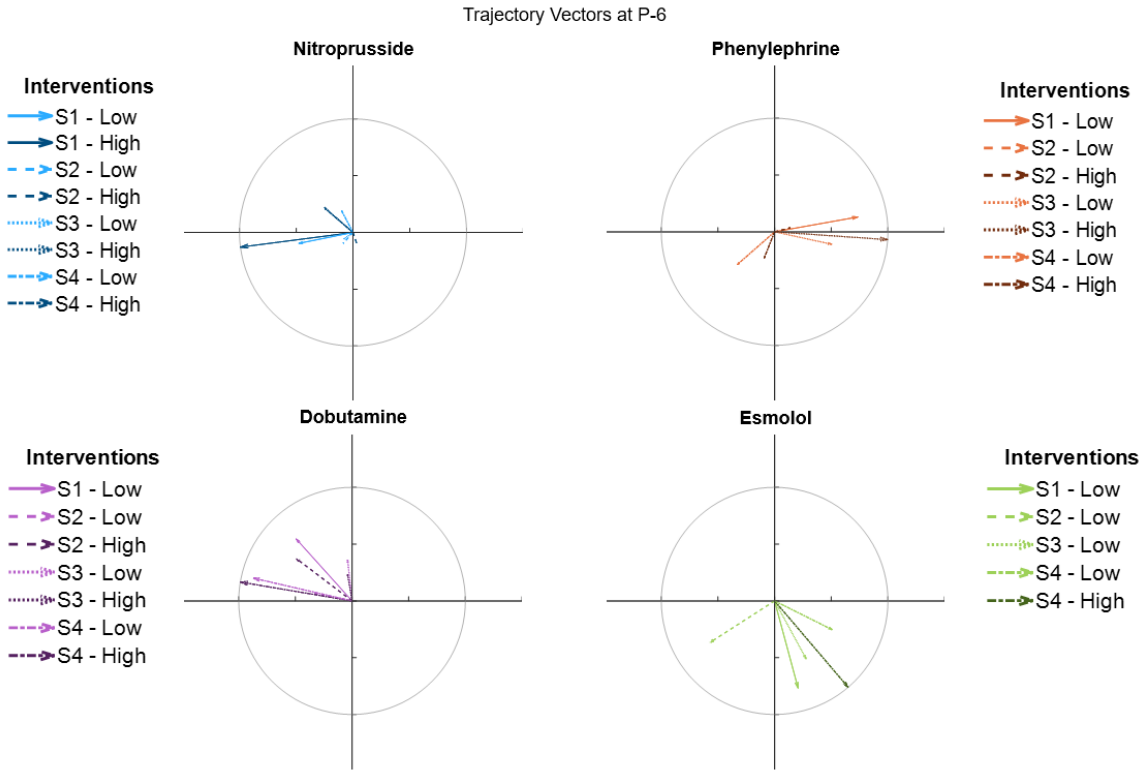

Figure 4-3: Trajectory vectors at P-6 categorized by pharmacological intervention. Vectors from all four animal studies are displayed.

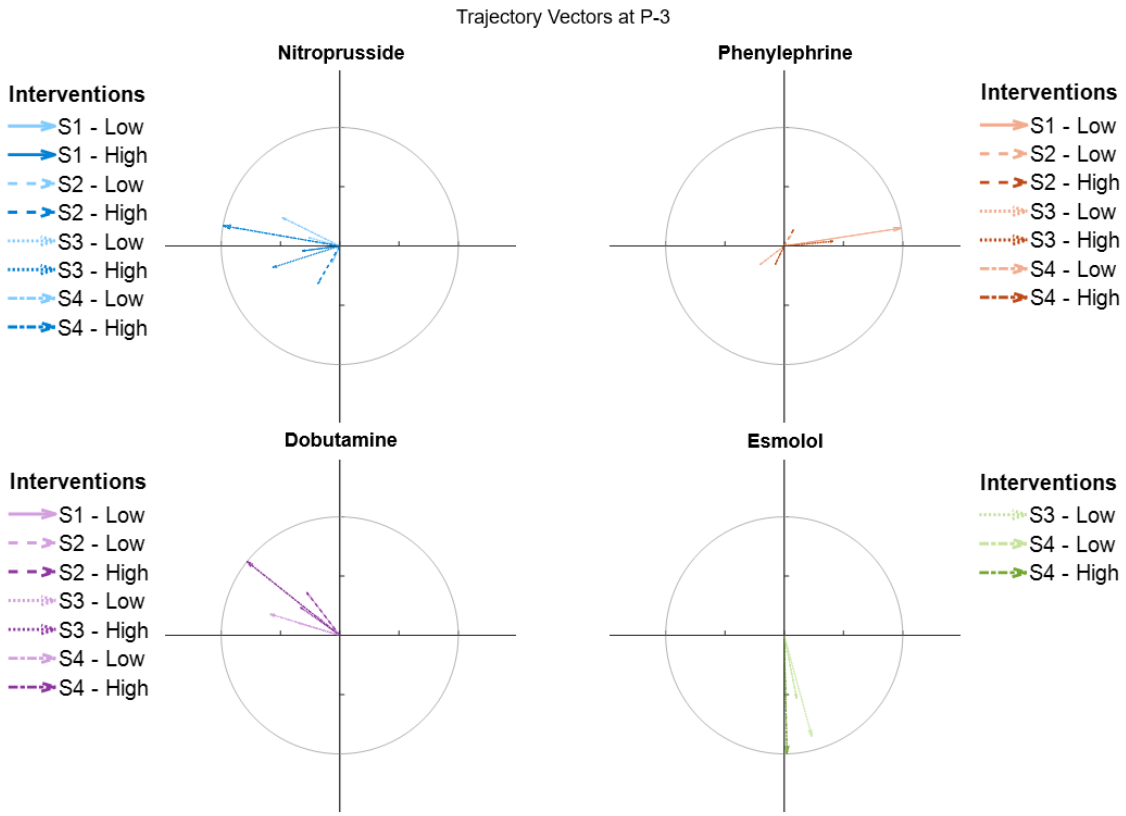

Figure 4-4: Trajectory vectors at P-3 categorized by pharmacological intervention. Vectors from all four animal studies are displayed.

4.0.3 Comparison of trajectory vector parameters to metrics from baseline and prior state

The magnitude and angle of each trajectory vector were compared to the Frank-Starling metrics of each corresponding baseline (Figures 4-5 and 4-6). This depiction of results allows us to assess the state dependency of the trajectory vector approach. Many hemodynamic metrics used in the clinic are influenced by underlying condition, complicating the selection of proper medical treatment for an individual. If no relationship between the parameters of the trajectory vector and baseline state exists, the approach can be utilized to detect consistent cardiac trends with pharmacological interventions and support devices.

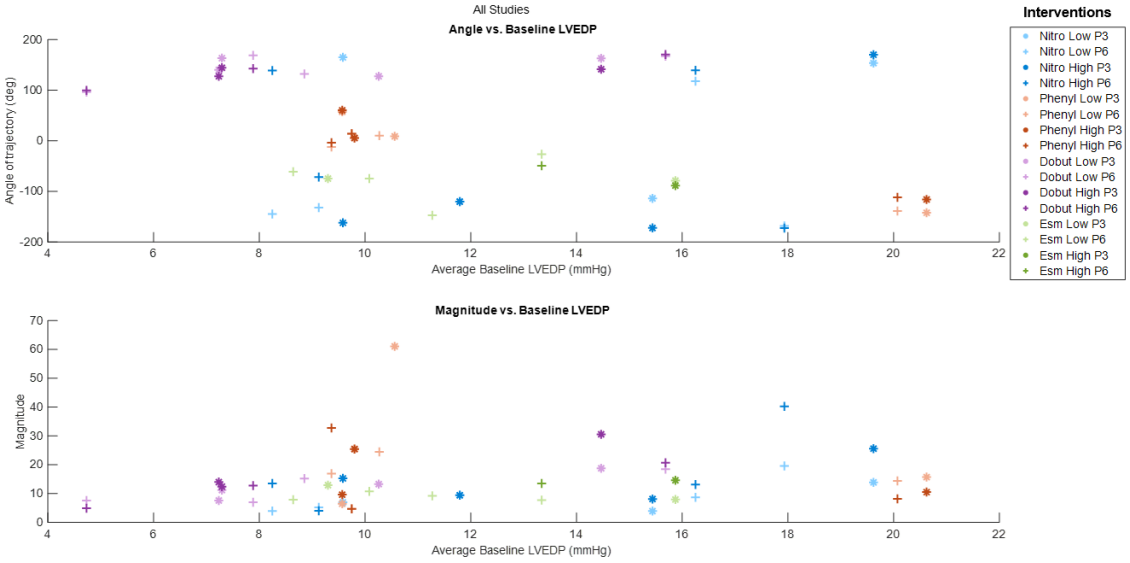

Figure 4-5: Comparison of trajectory magnitude and angle to baseline LVEDP. Vectors from all four animal studies are displayed.

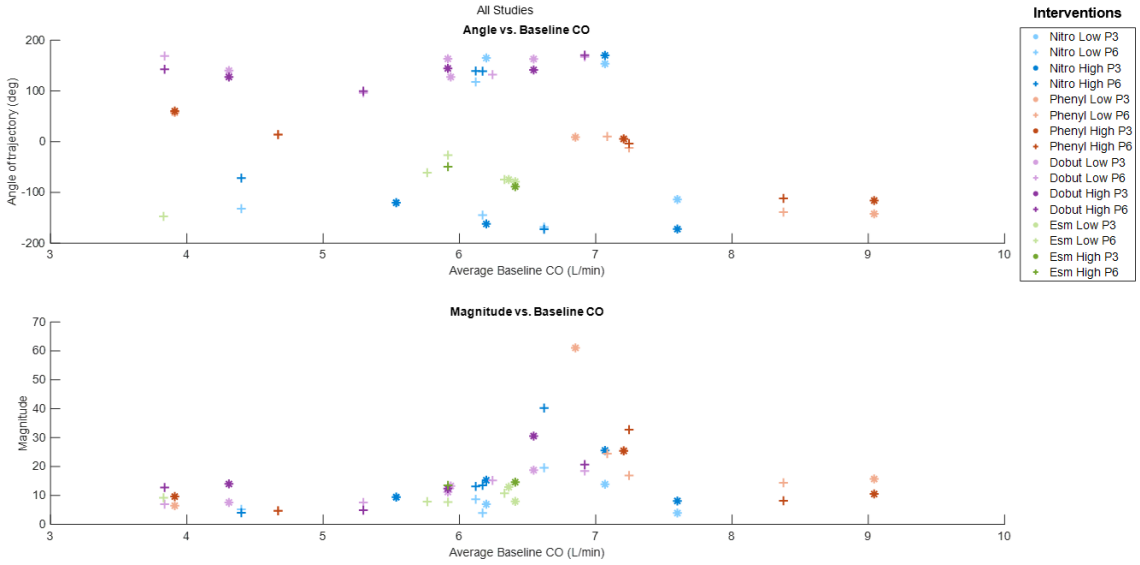

Figure 4-6: Comparison of trajectory magnitude and angle to baseline CO. Vectors from all four animal studies are displayed.

Prior state was also considered in the assessment of trajectory vector parameters as patient baseline may not always be known. Furthermore, in settings of continuous monitoring, clinicians sometimes can only rely on the most recent information gathered. Examining the progression of current state from prior state is critical in fully determining state dependency. Figures 4-7 and 4-8 use the relative dose response trajectory vectors to compare against prior state, as we are assessing stepped changes in response.

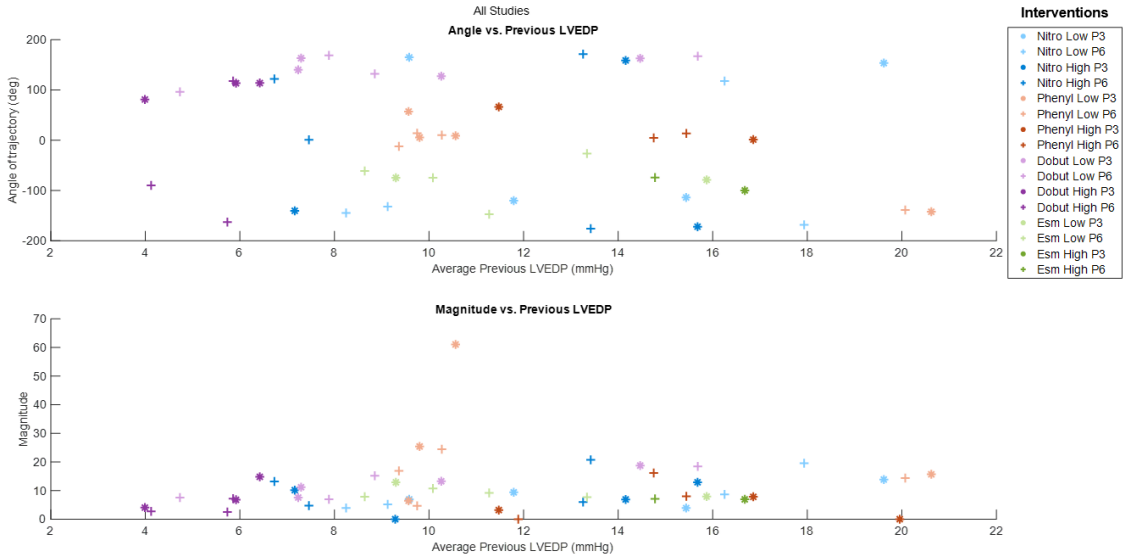

Figure 4-7: Comparison of trajectory magnitude and angle to previous LVEDP. Previous state is defined as baseline for the low dose vector and low dose for the high dose vector. Vectors from all four animal studies are displayed.

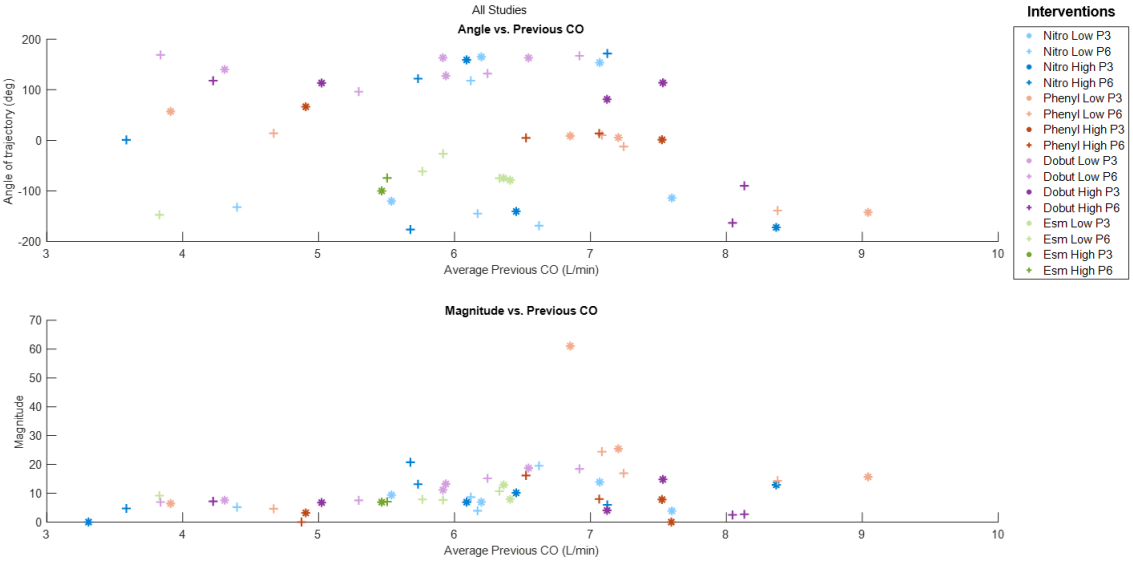

Figure 4-8: Comparison of trajectory magnitude and angle to previous CO. Previous state is defined as baseline for the low dose vector and low dose for the high dose vector. Vectors from all four animal studies are displayed.

Chapter 5

Discussion and Conclusions

5.1 Discussion of vector analysis results

To begin discussion of the vector analysis results, we refer back to the key questions proposed in Section 2.2 (Table 2.1).

5.1.1 Feasibility of the trajectory vector approach

The feasibility of the proposed trajectory vector approach to identify patterns among local variability can be validated by addressing the first three questions originally posed in Chapter 2 (Table 2.1), reiterated in Table 5.1. Their corresponding answers are also listed and will be explained in further detail below.

Table 5.1: Key questions and answers addressing the feasibility of the trajectory vector approach

Key Question	**Result**
Can progression of a cardiac state be monitored continuously?	**Yes.** Beat-to-beat points for three different cardiac states were evaluated in a 2D data representation.
Can significant physiological responses be differentiated from local physiological variation and measurement-related noise?	**Yes.** Consistent patterns among the trajectory vectors for each intervention were present across all animals.
Are drug responses independent of baseline state?	**Yes.** There is no correlation between vector angle or magnitude and baseline state.

Controlled hemodynamic data was successfully collected during all four animal studies across a few minutes of three different states, as evidenced in the Frank-

Starling representations in Appendix B. Data were collected continuously as an animal transitioned from its baseline state to a low dose and then a high dose state after the administration of a pharmacological intervention. Forming a 2D representation to assess the animal data proved to be advantageous, providing a higher resolution analysis of dynamic cardiac state. During the course of the studies, hemodynamic metrics were collected on separate channels as 1D variables, making it unclear whether fluctuations in the signals were within the normal bounds of the animal's physiology or were significant deviations caused by pharmacological intervention. By relating two variables commonly used to assess cardiac function along the same time scale, shifts in animal became much more apparent. Given the dependent relationship of cardiac performance on cardiac preload, using the Frank-Starling metrics allowed a much less ambiguous view of animal state.

The various filtering techniques applied, such as respiratory variation filtering, certainly eased the differentiation of drug responses from both measurement-related variation and inherent physiological variation. Separate animal states can be seen in Figures in Appendix B). More importantly, applying Gaussian mixture model clustering allowed specific patterns within the data to be identified and generated distinct trajectories for the drugs administered in the animal studies. Even within an individual animal state, such as the steady-state low dose effect, multiple normally distributed clusters can be detected (Figures 3-7a and 3-7b). Such granularity in the method can be useful to see even smaller physiological disturbances caused by cardiac events.

Arguably the most impactful topic of discussion, the question of the trajectory vector's state dependency is the last to be addressed. Although the direction of the trajectories for each intervention was consistent across animals (Figure 4-1), the drug responses may have been influenced by the filling pressures or cardiac output of the baseline state. Figures 4-5 and 4-6 compare the magnitude and angle of the vectors against baseline preload and cardiac performance. At first glance, there does not seem to be a correlation between the metrics defining baseline state and the parameters of the trajectory vectors. Rather than depending on baseline LVEDP and CO, the

direction of the trajectory vectors are grouped by type of pharmacological intervention, as shown by the clustering of points with similar colors in the plots depicting vector angle. For example, nitroprusside, denoted by blue, has trajectories with an angle of $147^\circ \pm 19^\circ$ or $-138^\circ \pm 33^\circ$, regardless of the initial filling pressure or cardiac output. Similar consistency can be seen with dobutamine ($\alpha = 142^\circ \pm 24^\circ$) and esmolol ($\alpha = -75^\circ \pm 35^\circ$). Even when comparing relative dose response to prior state metrics, there is no distinct trend, with angle grouped by intervention type (Figure 4-2). These findings indicate that the directional shifts in the performance-load relationship induced by these drug responses are independent of baseline or prior state. The state independence of the trajectory vector's direction is an extraordinary advancement in the clinical value of this approach. The approach has the potential to monitor patients with a diverse range of underlying conditions and comorbidities, using trajectories that are consistent across changing hemodynamic variables. Without the need for a known baseline, the vectors could be wielded for a dual purpose: as a possible diagnostic when viewing a patient's progression from their previous cardiac state and as a prognostic for reliably predicting future patient condition.

In the figures plotting vector magnitude against baseline or prior CO, the distribution of magnitudes is generally uniform between 0 and 10, assumed to be a result of the smaller doses administered during the studies, and evenly distributed across the different interventions, indicating state independence. Interestingly, the magnitude distribution over both baseline and prior cardiac output peaks at around 6.8 L/min (Figures 4-1 and 4-2). The underlying causes are unclear, considering this slightly bell-shaped distribution is present even with the different interventions and not pertaining to a particular drug. If this pattern is not due to normal variation among dose response or outliers from an individual study, the shape of this distribution may imply that the vector magnitude is only state independent at particular ranges of CO. Further statistical analysis should be conducted to see whether this distribution is significantly different than the variation one may normally see in these animals' cardiac states. An additional analysis relating these observed trends with the doses administered for each drug may also be beneficial to discover possible relationships.

In the future, larger data sets could be collected among the range of pharmacological agents administered to investigate this ambiguous pattern between trajectory vector magnitude and cardiac output.

It can be noted that the data collected during the phenylephrine intervention in VBU00221 produced trajectories that varied significantly in direction compared to the other vectors for the same drug, with the angle of its trajectory at an approximate 100° difference from the average of the other three studies. This is reflected in the bottom-right trajectory vector plot in Figure 4-1 and in the four data points grouped near the average baseline LVEDP of 20 mmHg (Figure 4-5) and average baseline CO of 8.5 L/min (Figure 4-6). This may be due to an adverse reaction to phenylephrine for that particular animal. Additionally, the animal's baseline LVEDP and CO before phenylephrine were relatively high compared to those of other animals, indicating that baseline state may have had an effect on drug response for this animal. While this seems to contradict our previous conclusion on the approach's state independence, perhaps the trajectory vector is only state independent within a certain range of baseline values for each intervention. Further investigation into the baseline physiology of the animal from VBU00221 should be conducted to better understand this discrepancy.

5.1.2 Capability of the trajectory vector approach

With the feasibility of the trajectory vector approach validated, the extent to which the approach is influenced by pharmacological intervention, Impella support level, and drug dose must be characterized, as stated in Table 5.2. The approach's capability to detect varying drug effect, dose, and Impella support, which is also shown in the table, is explained more thoroughly below.

When inspecting the resulting trajectory vectors of each pharmacological intervention in Figures 4-3 and 4-4, the directions reflect those of the predicted trajectories from Figure 2-8, with each drug effect correlating to a different shift in the performance-load relationship. Outlier angles for each intervention were removed using the default robust MATLAB algorithm of more than three scaled median absolute

Table 5.2: Key questions and answers addressing the capability of the trajectory vector approach

Key Question	Result
For a particular physiological state, what does the trajectory look like?	The trajectory vectors for each intervention aligned with the expected regions in the unit circle. Shifts in the performance-load relationship were seen in all four quadrants.
How does the level of Impella support affect the changes in state?	No consistent correlation was found between average vector magnitude or angle and p-level. Decreasing Impella support seemed to decrease variation in both magnitude and angle.
How does the dose of a drug affect the changes in state?	Vector magnitude is larger at higher dose level for the same drug and p-level.

deviations (MAD) away from the median. The resulting range of trajectory angles for each drug is depicted in Figure 5-1a. Two regions for phenylephrine are defined, with the bottom-left region representing the disparate response during VBU00221 and the top-right region representing the responses from the remaining three studies. The average angle and standard deviation for each intervention are also displayed in regions in Figure 5-1b, accounting for about 68% of the values from the same normal distribution. Excluding the outlier VBU00221 phenylephrine region, none of the intervention regions overlapped with one another except for nitroprusside. This inconsistency can be explained by nitroprusside having the largest amount of variation in direction, with $\sigma = 46.4°$, compared to the second largest variation of $\sigma = 24.0°$ in dobutamine. Nonetheless, with the diverse range of vasoactive and inotropic agents administered, the concomitant shifts in the performance-load relationship were unique, demonstrating the ability of the trajectory vector approach to detect changes across a spectrum of cardiac states.

No consistent trends were found with how level of Impella support influences the angle and magnitude of a trajectory vector, illustrating that the general direction or region of a pharmacological trajectory can be determined regardless of device interactions. However, for most of the drug interventions, there was a reduction in the variation present in magnitude (Figure 5-2) and angle (Figure 5-3) when Impella support was decreased, suggesting that the presence of device flow may introduce

more variation in physiological state. Consequently, the trajectory vector approach may not be the ideal monitoring tool for patients requiring high levels of Impella support, such as those with severe forms of cardiogenic shock. Caution must be taken to distinguish significant shifts in the performance-load relationship from these larger deviations in trajectory angle and magnitude. The trajectory metric could be more reliable as a diagnostic and prognostic for patients recovering from surgery and those in situations of device weaning.

The magnitude of a vector is generally larger during the high dose state than during the low dose state, for the same drug and p-level (Figure 5-4). The average magnitudes and their standard deviations for each drug intervention dose level are listed in Table 5.3. Through distinguishing dose responses for individual interventions, trajectory vectors can inform clinicians on titrating the appropriate initial amount and subsequent dose increments when administering pharmacological treatment for patients.

We emphasize that the above findings and discussion points are only relevant to the unique trajectory vector approach developed in this work, a newly developed computational model that has been trained on a specific data set. Future steps to further validate model fit and general application are outlined in a schematic in Figure 5-5. Here, the model in question is the trajectory vector approach. This work has completed the initial step of training the model on a Training Set, which in this case is the data set from the four controlled animal studies conducted. The model must be evaluated on a Validation Set, which would involve the same interventions and variables as the Training Set but with a larger sample size. Through statistical analyses comparing the distributions of the training trajectory vectors and the validation trajectory vectors, accuracy and repeatability of the approach can be defined. Based on these results, the model can be tweaked and retrained on the Training Set. The series of steps above are repeated until the best-performing model is found. This optimal model is finally confirmed through a separate Test Set, such as unlabeled animal data or labeled clinical patient data, to ensure reproducible results.

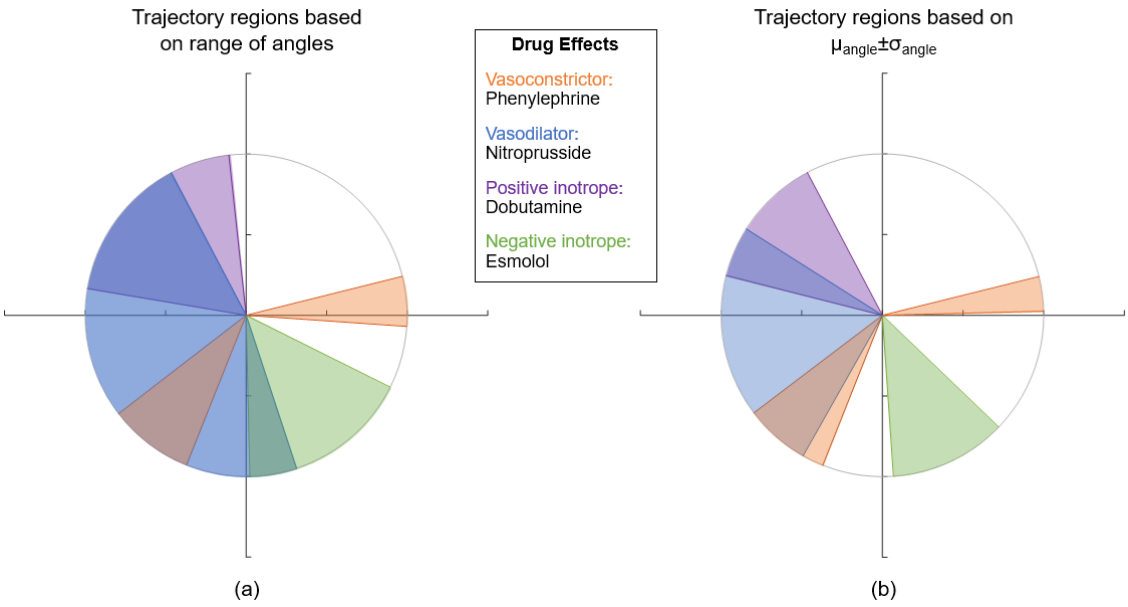

Figure 5-1: Trajectory regions based on angle range, mean, and standard deviation. Outliers were removed using the default MATLAB `rmoutliers` function. There are two regions for phenylephrine, with the left-sided region representing the disparate response during VBU00221 and the right-sided region representing the responses from the remaining three studies. (a) Left-sided phenylephrine range: $\alpha = [-142.4°, -111.7°]$, Right-sided phenylephrine range: $\alpha = [-4.0°, 14.0°]$, Nitroprusside range: $\alpha = [117.8°, 288.2°]$, Dobutamine range: $\alpha = [96.2°, 170.4°]$, Esmolol range: $\alpha = [-88.7°, -26.5°]$. (b) Left-sided phenylephrine region: $\mu \pm \sigma = -127.2° \pm 15.6°$, Right-sided phenylephrine region: $\mu \pm \sigma = 7.7° \pm 6.2°$, Nitroprusside region: $\mu \pm \sigma = 194.1° \pm 46.4°$, Dobutamine region: $\mu \pm \sigma = 141.7° \pm 24.0°$, Esmolol region: $\mu \pm \sigma = -64.9° \pm 21.1°$.

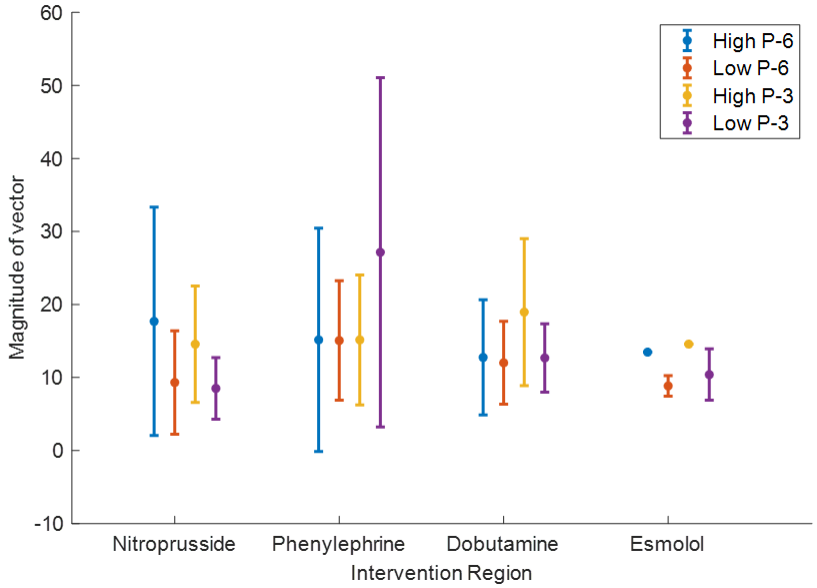

Figure 5-2: Comparison of trajectory vector magnitude and p-level. For each drug, magnitude was sorted by dose and p-level. Points represent average magnitude and error bars represent ± one standard deviation. For most interventions, for the same dose, reducing p-level resulted in a reduction in magnitude variation.

Table 5.3: Average magnitudes and standard deviations of trajectory vectors sorted by drug and dose

Drug	Dose	*n*	$\mu_{magnitude}$	$\sigma_{magnitude}$
Nitroprusside	Low	8	8.8	6.0
	High	8	17	12
Phenylephrine	Low	8	21	18
	High	6	15	11
Dobutamine	Low	8	12	4.8
	High	6	16	8.8
Esmolol	Low	6	9.4	2.1
	High	2	14	.78

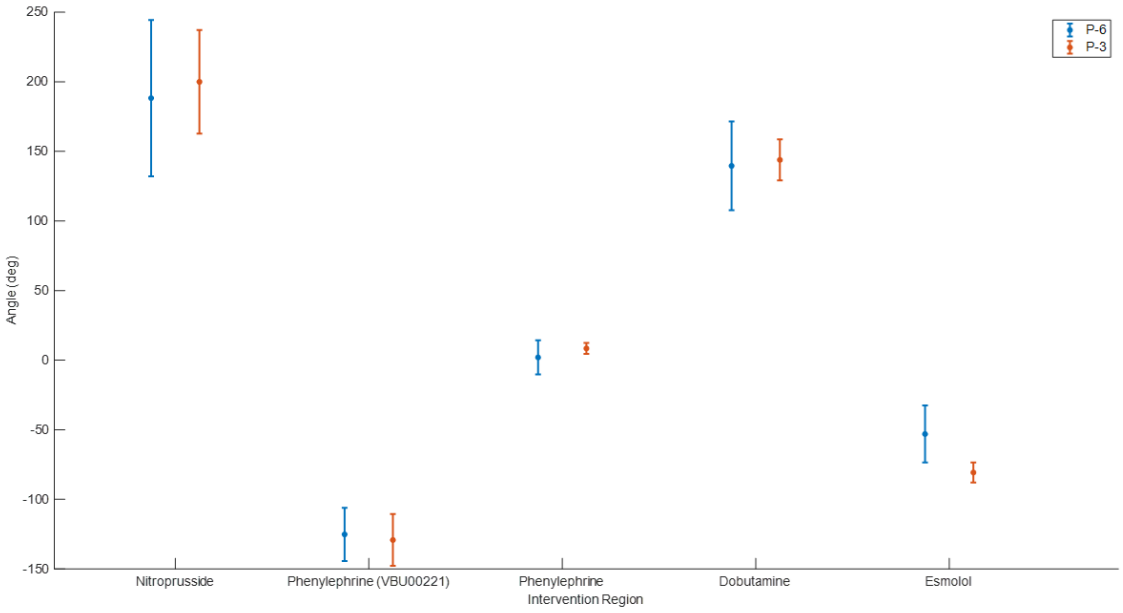

Figure 5-3: Comparison of trajectory vector angle and p-level. For each drug, angle was sorted by p-level. Points represent average magnitude and error bars represent ± one standard deviation. There are two data sets for phenylephrine, with the first set representing the disparate response during VBU00221 and the right-sided region representing the responses from the remaining three studies. For most interventions, reducing p-level resulted in a reduction in angle variation.

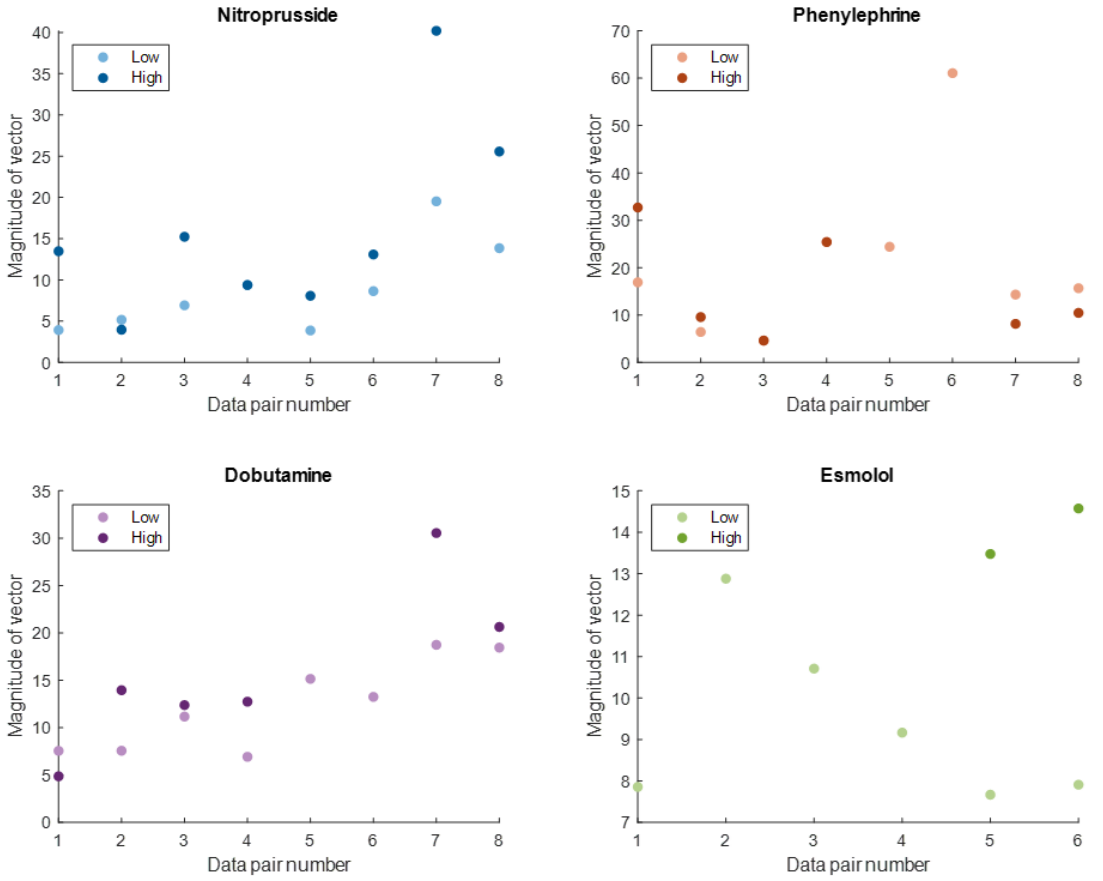

Figure 5-4: Comparison of trajectory vector magnitude and dose level. Each pair of data points is taken at the same p-level, animal state, and study. For most data points, the higher dose produced a larger magnitude trajectory vector.

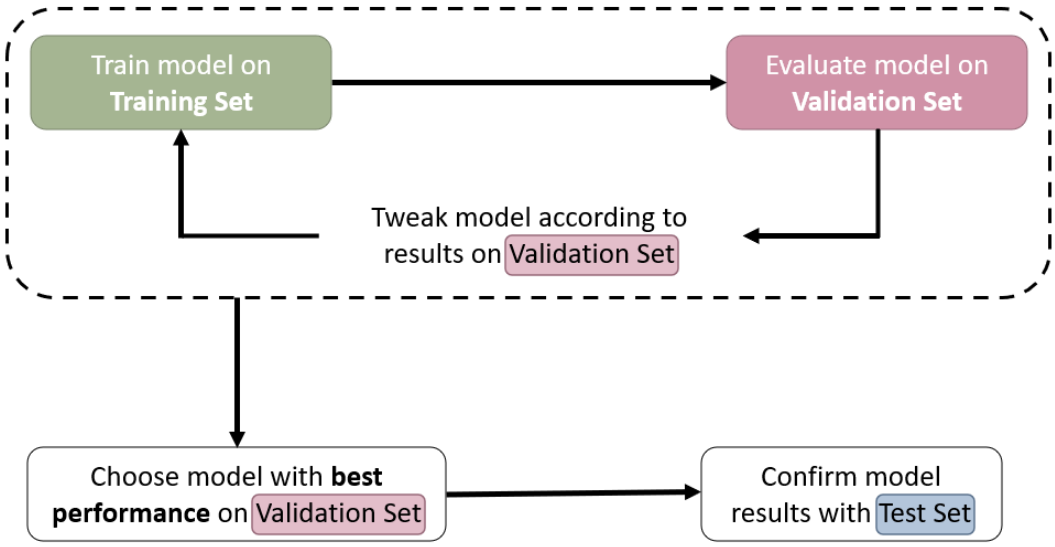

Figure 5-5: Schematic of the training, validation, and test process for a model. Here, the model in question is the trajectory vector approach. The approach is trained on a Training Set, which in this case is the data set from the four controlled animal studies conducted. Then the model must be evaluated on a Validation Set, which would involve the same interventions and variables as the Training Set but with a larger sample size. Through statistical analyses comparing the distributions of the training trajectory vectors and the validation trajectory vectors, accuracy and repeatability of the approach can be defined. Based on these results, the model can be tweaked and retrained on the Training Set. The series of steps above are repeated until the best-performing model is found. This optimal model is finally confirmed through a separate Test Set, such as unlabeled animal data or labeled clinical patient data, to ensure reproducible results.

5.2 Limitations

There are several limitations of this work regarding the animal model used and the study protocol developed. The protocol solely relied on using a healthy animal model to test feasibility of the trajectory vector approach. However, in the traditional use case of the Impella CP, the patient is undergoing cardiogenic shock. To further validate this approach, baseline and pharmacological intervention data must be collected during an acute cardiogenic shock animal model as well. The protocol also only included two categories of drug dose and Impella support levels. Diving deeper into how these variables influence the characterization of a trajectory vector will require data collection at additional doses and p-levels. Lastly, the sample size was small (n=4). Additional studies with similar sample size or a study with a significantly larger sample size should be conducted to confirm the trends seen in this work, especially given the amount of variability present in native physiological state.

The variation in the measurements of cardiovascular metrics could have introduced sources of error in the data. The PV catheter in the left ventricle was subjected to changes in contractility due to the natural cardiac cycle as well as the pharmacological interventions, displacing the electrodes on the tip and making the LVV signal unreliable. Although the LVV signal was calibrated at the baseline, low dose, and high dose states for every drug, slight changes in the signal during these states may have been unaccounted for. Thermodilution was used to calibrate the LVV signal. Despite thermodilution being a widely accepted method of measuring cardiac output in the clinic, the produced measurements are highly variable and require averaging of multiple measurements to result in potentially inaccurate calculations [12]. Using thermodilution as the gold standard for volume calibration may have introduced further variability when extracting beat-to-beat CO for the Frank-Starling interpretation. Local cardiac arrhythmias, premature ventricular contractions, and other abnormalities in the EKG signal may have also introduced error in the identification of beat-to-beat LVEDP, as the technique relies on correlating the occurrence of end diastole to the QRS complex.

While the method of Gaussian mixture model clustering was carefully selected among other available clustering options, there are a few limitations to this technique. GMM clustering requires the number of clusters before model fitting, which can often influence the resulting optimal model. In most applications, the number of clusters within a data set is unknown, so it may be difficult to estimate this parameter. The k-means++ algorithm can guide how the centroids of cluster should be initialized, which can be considered as an initial condition when applying GMM clustering. Similarly, since the controlled data set under analysis is labeled by state, the data points within each state can be used as initial cluster assignments to guide the optimal Gaussian mixture model fit. These techniques may also be able to produce more consistent model fitting, as GMM clustering is sensitive to initial conditions and may converge to a local optimum. Additionally, only the two most popular criteria were used to evaluate the fitted GMMs. Other evaluation criteria that may be more appropriate for determining the optimal model should be considered in the future.

5.3 Conclusions

Cardiogenic shock is a life-threatening condition traditionally characterized by high filling pressures and low cardiac output. Treatment and management of CS relies on using accurate hemodynamic metrics to guide the titration of mechanical circulatory support devices. Even with recent innovation of MCS technology resulting in a rising prevalence of percutaneous ventricular assist devices, there remains limited evidence supporting device usage for patients with CS. Current studies analyzing trends in pVAD usage suggest a lack of proper diagnostic metrics to guide titration of these devices to the appropriate patient population [14][41]. The current clinical standard for monitoring hemodynamic state, i.e. the pulmonary artery catheter, has multiple shortcomings, including noncontinuous sampling, inaccurate assumption of parameters, and issues with deployment. As follows, there lies opportunity to develop a more informative, direct, and reliable metric to help clinicians characterize patient state.

In this work, we present a novel approach to both qualitatively and quantitatively

characterize dynamic changes in cardiac state. Through a series of controlled animal studies, we collect hemodynamic data during baseline and various pharmacological interventions, at varying doses and Impella support levels. Using a 2D performance-load representation not unlike the Frank-Starling association, we employ Gaussian mixture model clustering to identify distinct patterns in an animal's drug response. We generate trajectory vectors, parameterized by angle and magnitude, for each drug effect, and further categorize them by drug dose and Impella support level. Findings suggest feasibility of the trajectory vector approach to identify shifts of the performance-load relationship, showing that various pharmacological effects are independent of baseline state. We can leverage the reliability of the trajectory's pattern identification to generalize this approach for a range of patient states in the clinic. Results also indicate the approach can distinguish intervention dose levels, with minimal influences from the level of Impella support, expanding the potential utility of this approach to inform treatment options for cardiogenic shock.

Near-future work includes analysis of additional metrics to inform the extent of the trajectory vector approach's capability. Extracting the slope of the end-systolic pressure-volume relationship during the IVC occlusions performed during the studies can quantify contractility for the various pharmacological interventions used. With a correlation between contractility and drug dose for a particular intervention, the vector may be used to reliably characterize and predict a specific contractile state. Further exploration of available clustering methods is needed to find the most appropriate technique for optimizing the trajectory vector method. One alternative method to Gaussian mixture model clustering is maximum a-posteriori Dirichlet process mixtures (MAP-DP), developed by Raykov et al [42]. Rather than requiring a specified number of clusters k to assign groups, MAP-DP infers k from the unlabeled data itself, making it advantageous for applications in which the number of significant trends is unknown. The ability to identify cardiac events or changes in cardiac behavior without knowledge of timing is imperative for the clinical utility of the trajectory vector approach. Current methods rely on data collected during planned state changes in an animal. Next steps involve characterizing continuous sections of data,

such as the transition between states, through clustering.

Longer term work consists of investigating the latter two key questions proposed in the Introduction. Applying the techniques formulated in this thesis to the Impella-derived performance-load metrics proven in previous work can simulate the use case of the trajectory vector approach in the clinic. The ability to predict trajectories can be developed through machine learning techniques, such as training the approach on controlled animal data sets and testing its accuracy and repeatability on unlabeled animal data sets. Similar techniques could be expanded to analysis of human patient data sets, as well as real-time data analysis, for translation from computational bench to hospital bedside.

References

[1] Aditya Mandawat and Sunil V. Rao. Percutaneous mechanical circulatory support devices in cardiogenic shock. *Circulation: Cardiovascular Interventions*, 10(5):e004337, 2017.

[2] Dhaval Kolte, Sahil Khera, Wilbert S. Aronow, Marjan Mujib, Chandrasekar Palaniswamy, Sachin Sule, Diwakar Jain, William Gotsis, Ali Ahmed, William H. Frishman, and Gregg C. Fonarow. Trends in incidence, management, and outcomes of cardiogenic shock complicating st‐elevation myocardial infarction in the united states. *Journal of the American Heart Association*, 3(1):e000590, 2014.

[3] Sean van Diepen, Jason N. Katz, Nancy M. Albert, Timothy D. Henry, Alice K. Jacobs, Navin K. Kapur, Ahmet Kilic, Venu Menon, E. Magnus Ohman, Nancy K. Sweitzer, Holger Thiele, Jeffrey B. Washam, and Mauricio G. Cohen. Contemporary management of cardiogenic shock: A scientific statement from the american heart association. *Circulation*, 136(16):e232–e268, 2017.

[4] Leonard S. Lilly. *Pathophysiology of Heart Disease: A Collaborative Project of Medical Students and Faculty*. Wolters Kluwer/Lippincott Williams & Wilkins, Baltimore, MD, fifth edition, 2011.

[5] Umesh K Gidwani and Sunny Goel. The pulmonary artery catheter in 2015: The swan and the phoenix. *Cardiol. Rev.*, 24(1):1–13, January 2016.

[6] Kevin Ikuta, Yun Wang, Austin Robinson, Tariq Ahmad, Harlan M. Krumholz, and Nihar R. Desai. National Trends in Use and Outcomes of Pulmonary Artery Catheters Among Medicare Beneficiaries, 1999-2013. *JAMA Cardiology*, 2(8):908–913, 08 2017.

[7] Jr Connors, Alfred F., Theodore Speroff, Neal V. Dawson, Charles Thomas, Jr Harrell, Frank E., Douglas Wagner, Norman Desbiens, Lee Goldman, Albert W. Wu, Robert M. Califf, Jr Fulkerson, William J., Humberto Vidaillet, Steven Broste, Paul Bellamy, Joanne Lynn, and William A. Knaus. The Effectiveness of Right Heart Catheterization in the Initial Care of Critically III Patients. *JAMA*, 276(11):889–897, 09 1996.

[8] Renda Soylemez Wiener and H. Gilbert Welch. Trends in the Use of the Pulmonary Artery Catheter in the United States, 1993-2004. *JAMA*, 298(4):423–429, 07 2007.

[9] The ESCAPE Investigators and ESCAPE Study Coordinators*. Evaluation Study of Congestive Heart Failure and Pulmonary Artery Catheterization EffectivenessThe ESCAPE Trial. *JAMA*, 294(13):1625–1633, 10 2005.

[10] Clyde W. Yancy, Mariell Jessup, Biykem Bozkurt, Javed Butler, Donald E. Casey, Mark H. Drazner, Gregg C. Fonarow, Stephen A. Geraci, Tamara Horwich, James L. Januzzi, Maryl R. Johnson, Edward K. Kasper, Wayne C. Levy, Frederick A. Masoudi, Patrick E. McBride, John J.V. McMurray, Judith E. Mitchell, Pamela N. Peterson, Barbara Riegel, Flora Sam, Lynne W. Stevenson, W.H. Wilson Tang, Emily J. Tsai, and Bruce L. Wilkoff. 2013 accf/aha guideline for the management of heart failure: Executive summary. *Circulation*, 128(16):1810–1852, 2013.

[11] R D Brandstetter, G R Grant, M Estilo, F Rahim, K Singh, and B Gitler. Swan-Ganz catheter: misconceptions, pitfalls, and incomplete user knowledge–an identified trilogy in need of correction. *Heart Lung*, 27(4):218–222, July 1998.

[12] Paul E Marik. Obituary: pulmonary artery catheter 1970 to 2013. *Ann. Intensive Care*, 3(1):38, November 2013.

[13] Karl Werdan, Stephan Gielen, Henning Ebelt, and Judith S. Hochman. Mechanical circulatory support in cardiogenic shock. *European Heart Journal*, 35(3):156–167, 09 2013.

[14] Ole Kristian Lerche Helgestad, Jakob Josiassen, Christian Hassager, Lisette Okkels Jensen, Lene Holmvang, Nanna Louise Junker Udesen, Henrik Schmidt, Hanne Berg Ravn, and Jacob Eifer Moller. Contemporary trends in use of mechanical circulatory support in patients with acute mi and cardiogenic shock. *Open Heart*, 7(1), 2020.

[15] Rohan Khera, Peter Cram, Xin Lu, Ankur Vyas, Alicia Gerke, Gary E. Rosenthal, Phillip A. Horwitz, and Saket Girotra. Trends in the Use of Percutaneous Ventricular Assist Devices: Analysis of National Inpatient Sample Data, 2007 Through 2012. *JAMA Internal Medicine*, 175(6):941–950, 06 2015.

[16] Abiomed, Danvers, MA. *Impella CP with SmartAssist for Use During Cardiogenic Shock and High-Risk PCI: Instructions for Use and Clinical Reference Manual*, July 2020.

[17] Brian Y Chang, Steven P Keller, Sonya S Bhavsar, Noam Josephy, and Elazer R Edelman. Mechanical circulatory support device-heart hysteretic interaction can predict left ventricular end diastolic pressure. *Sci. Transl. Med.*, 10(430):eaao2980, February 2018.

[18] Steven P Keller, Brian Y Chang, Qing Tan, Zhengyang Zhang, Ahmad El Katerji, and Elazer R Edelman. Dynamic modulation of device-arterial coupling to determine cardiac output and vascular resistance. *Ann. Biomed. Eng.*, 48(9):2333–2342, September 2020.

[19] Martin Ester, Hans-Peter Kriegel, Jörg Sander, and Xiaowei Xu. A density-based algorithm for discovering clusters in large spatial databases with noise. In *Proceedings of the Second International Conference on Knowledge Discovery and Data Mining*, KDD'96, page 226–231. AAAI Press, 1996.

[20] AC Dornhorst, P Howard, and GL Leathart. Respiratory variations in blood pressure. *Circulation*, 6(4):553–558, 1952.

[21] Hooman Sedghamiz. Matlab implementation of pan tompkins ecg qrs detector., 03 2014.

[22] Jiapu Pan and Willis J. Tompkins. A real-time qrs detection algorithm. *IEEE Transactions on Biomedical Engineering*, BME-32(3):230–236, 1985.

[23] M. M. Swindle, A. Makin, A. J. Herron, Jr F. J. Clubb, and K. S. Frazier. Swine as models in biomedical research and toxicology testing. *Veterinary Pathology*, 49(2):344–356, 2012. PMID: 21441112.

[24] Christopher B. Overgaard and Vladimír Džavík. Inotropes and vasopressors. *Circulation*, 118(10):1047–1056, 2008.

[25] M Takeuchi, Y Igarashi, S Tomimoto, M Odake, T Hayashi, T Tsukamoto, K Hata, H Takaoka, and H Fukuzaki. Single-beat estimation of the slope of the end-systolic pressure-volume relation in the human left ventricle. *Circulation*, 83(1):202–212, 1991.

[26] Razvan O. Mada, Peter Lysyansky, Ana M. Daraban, Jürgen Duchenne, and Jens-Uwe Voigt. How to define end-diastole and end-systole?: Impact of timing on strain measurements. *JACC: Cardiovascular Imaging*, 8(2):148–157, 2015.

[27] Jörg Sander, Martin Ester, Hans-Peter Kriegel, and Xiaowei Xu. Density-based clustering in spatial databases: The algorithm gdbscan and its applications. *Data Mining and Knowledge Discovery*, 2(2):169–194, Jun 1998.

[28] Erich Schubert, Jörg Sander, Martin Ester, Hans Peter Kriegel, and Xiaowei Xu. Dbscan revisited, revisited: Why and how you should (still) use dbscan. 42(3), jul 2017.

[29] Peter J. Rousseeuw. Silhouettes: A graphical aid to the interpretation and validation of cluster analysis. *Journal of Computational and Applied Mathematics*, 20:53–65, 1987.

[30] Christopher Williams and Carl Rasmussen. Gaussian processes for regression. In D. Touretzky, M.C. Mozer, and M. Hasselmo, editors, *Advances in Neural Information Processing Systems*, volume 8. MIT Press, 1995.

[31] K G Joreskog. A general method for analysis of covariance structures. *Biometrika*, 57(2):239, August 1970.

[32] MathWorks. Cluster using gaussian mixture model.

[33] H Akaike. A new look at the statistical model identification. *IEEE Trans. Automat. Contr.*, 19(6):716–723, December 1974.

[34] Gideon Schwarz. Estimating the dimension of a model. *The Annals of Statistics*, 6(2):461–464, 1978.

[35] P. Stoica and Y. Selen. Model-order selection: a review of information criterion rules. *IEEE Signal Processing Magazine*, 21(4):36–47, 2004.

[36] Jouni Kuha. Aic and bic: Comparisons of assumptions and performance. *Sociological Methods & Research*, 33(2):188–229, 2004.

[37] Ritei Shibata. Selection of the order of an autoregressive model by akaike's information criterion. *Biometrika*, 63(1):117–126, 1976.

[38] E. J. Hannan and B. G. Quinn. The determination of the order of an autoregression. *Journal of the Royal Statistical Society. Series B (Methodological)*, 41(2):190–195, 1979.

[39] Michael Friendly, Georges Monette, and John Fox. Elliptical Insights: Understanding Statistical Methods through Elliptical Geometry. *Statistical Science*, 28(1):1 – 39, 2013.

[40] University of Utah Computer Science Department. How to draw a covariance error ellipse?

[41] K. Ergle, P. Parto, and S. R. Krim. Percutaneous Ventricular Assist Devices: A Novel Approach in the Management of Patients With Acute Cardiogenic Shock. *Ochsner J*, 16(3):243–249, 2016.

[42] Yordan P. Raykov, Alexis Boukouvalas, Fahd Baig, and Max A. Little. What to do when k-means clustering fails: A simple yet principled alternative algorithm. *PLOS ONE*, 11(9):1–28, 09 2016.

Appendix A

Supplementary Tables

Table A.1: Drug Interventions for VBU00202 (weight = 83.5 kg)

Drug	Concentration (mcg/mL)	Bolus (mL)	Total volume administered (mL)	State	Dose (mcg/kg/min)	Target hemodynamic metric
Nitroprusside	100	1	74			
				Low	0.25	MAP decrease ≥ 10 mmHg or MAP = 60 mmHg
				High	2.5	MAP decrease ≥ 10 mmHg or MAP = 60 mmHg
Phenylephrine	100	0.5	113			
				Low	2	MAP increase ≥ 10 mmHg or MAP = 110 mmHg
				High	N/A	
Dobutamine	100	1	185			
				Low	3	MAP increase ≥ 10 mmHg or HR increase ≥ 10 bpm
				High	N/A	
Esmolol	3200	1.5	265.8			
				Low	100	MAP decrease ≥ 10 mmHg or HR decrease ≥ 10 bpm
				High	N/A	

Table A.2: Drug Interventions for VBU00203 (weight = 68.1 kg)

Drug	Concentration (mcg/mL)	Bolus (mL)	Total volume administered (mL)	State	Dose (mcg/kg/min)	Target hemodynamic metric
Nitroprusside	100	0.5	27.6			
				Low	1	MAP decrease ≥ 10 mmHg or MAP = 60 mmHg
				High	2	MAP decrease ≥ 10 mmHg or MAP = 60 mmHg
Phenylephrine	100	0.5	33.6			
				Low	1	MAP increase ≥ 10 mmHg or MAP = 110 mmHg
				High	2	MAP increase ≥ 10 mmHg or MAP = 110 mmHg
Dobutamine	100	0.5	77.6			
				Low	1	HR increase ≥ 10 bpm or MAP increase ≥ 10 mmHg
				High	2.5	HR increase ≥ 10 bpm, MAP increase ≥ 10 mmHg, or MAP = 110 mmHg
Esmolol	3200	0.5	178			
				Low	150	MAP decrease ≥ 10 mmHg or HR decrease ≥ 10 bpm
				High	N/A	

Table A.3: Drug Interventions for VBU00205 (weight = 77 kg)

Drug	Concentration (mcg/mL)	Bolus (mL)	Total volume administered (mL)	State	Dose (mcg/kg/min)	Target hemodynamic metric
Nitroprusside	100	0.5	36.4			
				Low	0.5	MAP decrease ≥ 10 mmHg or MAP = 60 mmHg
				High	2	MAP decrease ≥ 10 mmHg or MAP = 60 mmHg
Phenylephrine	100	0.5	42			
				Low	1	MAP increase ≥ 10 mmHg or MAP = 110 mmHg
				High	2	MAP increase ≥ 10 mmHg or MAP = 110 mmHg
Dobutamine	100	0.5	149			
				Low	3	HR increase ≥ 10 bpm or MAP increase ≥ 10 mmHg
				High	3.5	HR increase ≥ 10 bpm, MAP increase ≥ 10 mmHg, or MAP = 110 mmHg
Esmolol	3200	0.5	98			
				Low	150	MAP decrease ≥ 10 mmHg or HR decrease ≥ 10 bpm
				High	N/A	

Table A.4: Drug Interventions for VBU00221 (weight = 83.9 kg)

Drug	Concentration (mcg/mL)	Bolus (mL)	Total volume administered (mL)	State	Dose (mcg/kg/min)	Target hemodynamic metric
Nitroprusside	100	0.5	43.7			
				Low	0.5	MAP decrease ≥ 10 mmHg or MAP = 60 mmHg
				High	2	MAP decrease ≥ 10 mmHg or MAP = 60 mmHg
Phenylephrine	100	0.5	45.3			
				Low	1	MAP increase ≥ 10 mmHg or MAP = 110 mmHg
				High	2	MAP increase ≥ 10 mmHg or MAP = 110 mmHg
Dobutamine	100	0.5	83			
				Low	1.5	HR increase ≥ 10 bpm or MAP increase ≥ 10 mmHg
				High	2.5	HR increase ≥ 10 bpm, MAP increase ≥ 10 mmHg, or MAP = 110 mmHg
Esmolol	3200	0.5	132.6			
				Low	100	MAP decrease ≥ 10 mmHg or HR decrease ≥ 10 bpm
				High	200	MAP decrease ≥ 10 mmHg, HR decrease ≥ 10 bpm, or MAP = 60 mmHg

Appendix B

Supplementary Figures

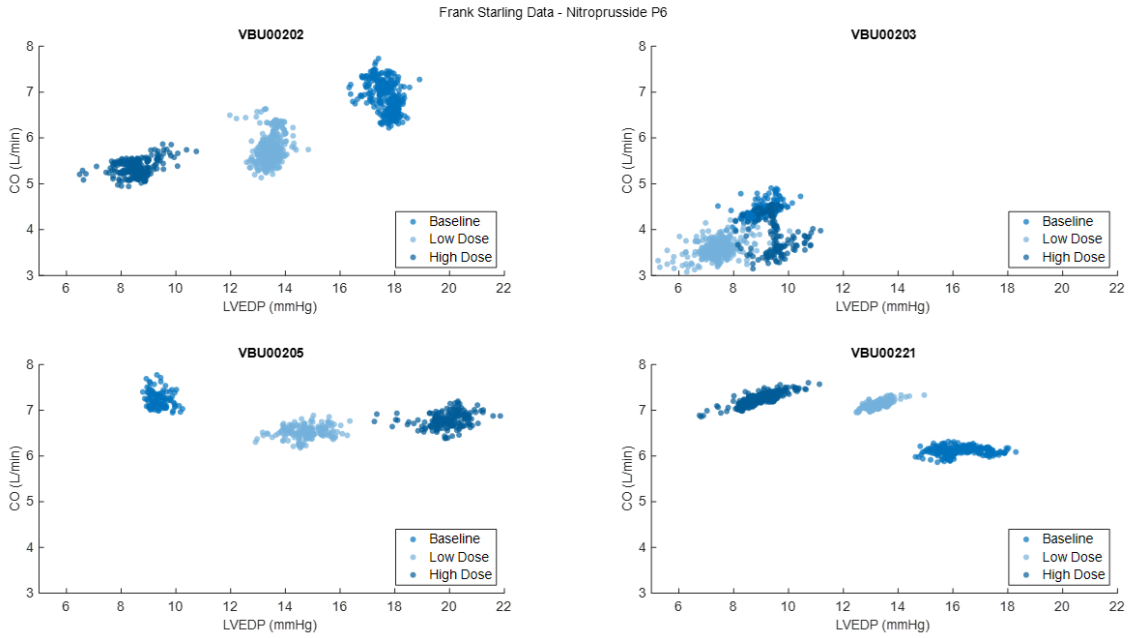

Figure B-1: Frank-Starling representation of nitroprusside at P-6 across all animals

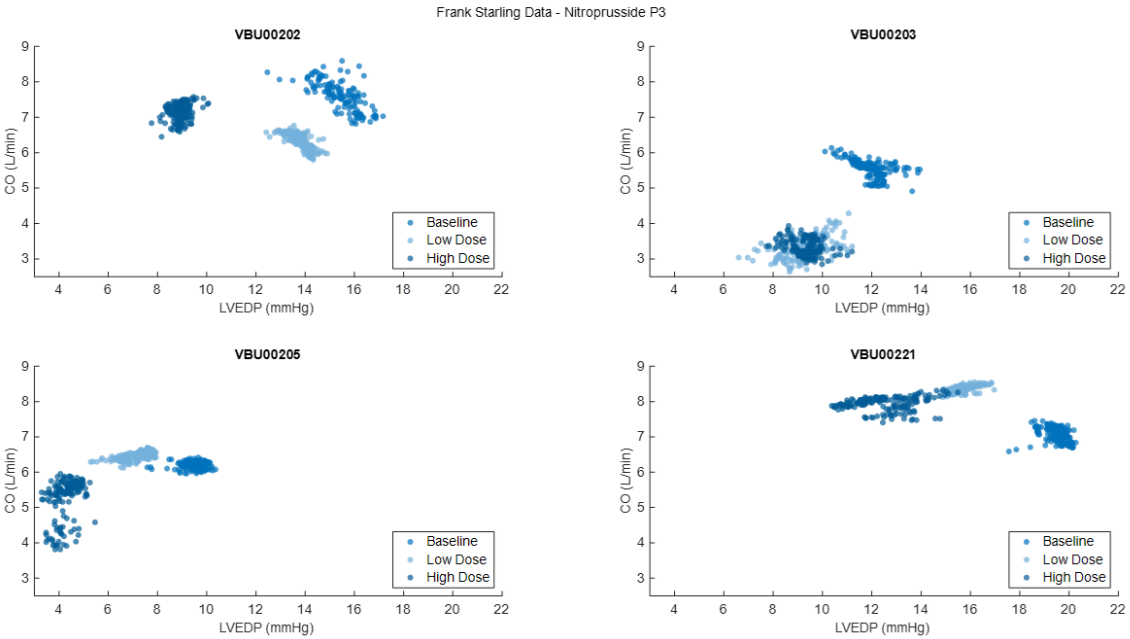

Figure B-2: Frank-Starling representation of nitroprusside at P-3 across all animals

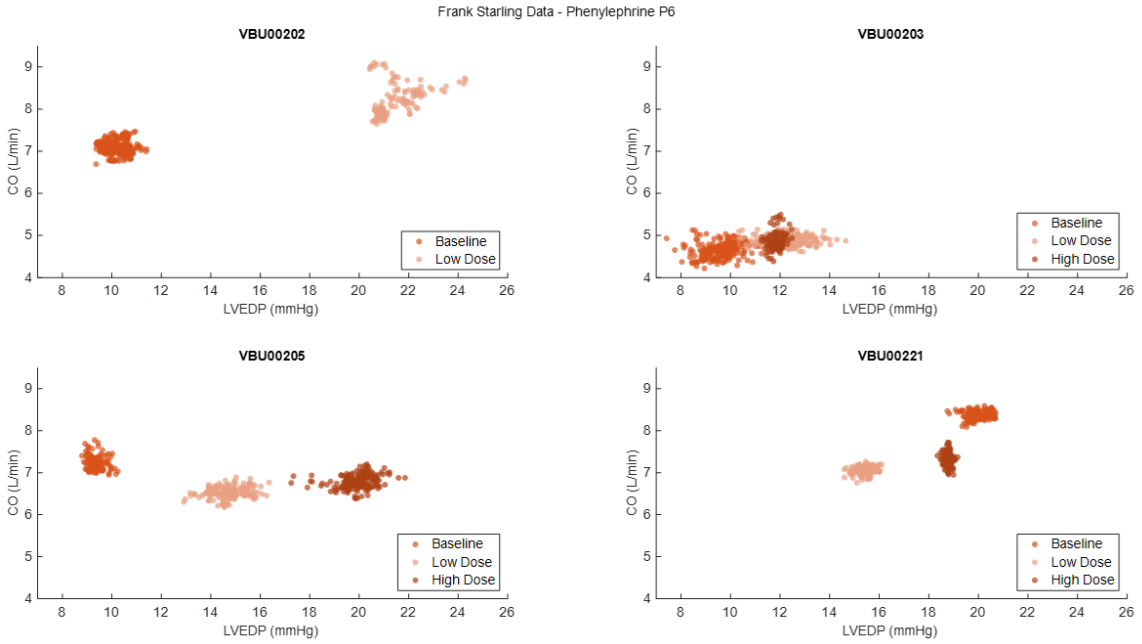

Figure B-3: Frank-Starling representation of phenylephrine at P-6 across all animals

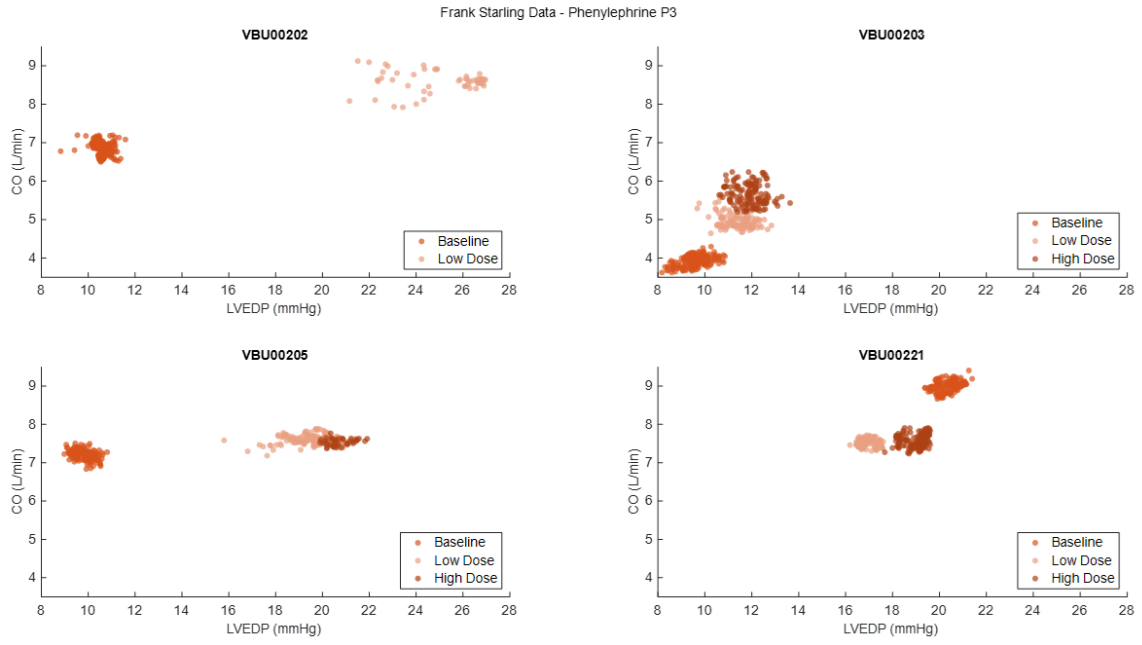

Figure B-4: Frank-Starling representation of phenylephrine at P-3 across all animals

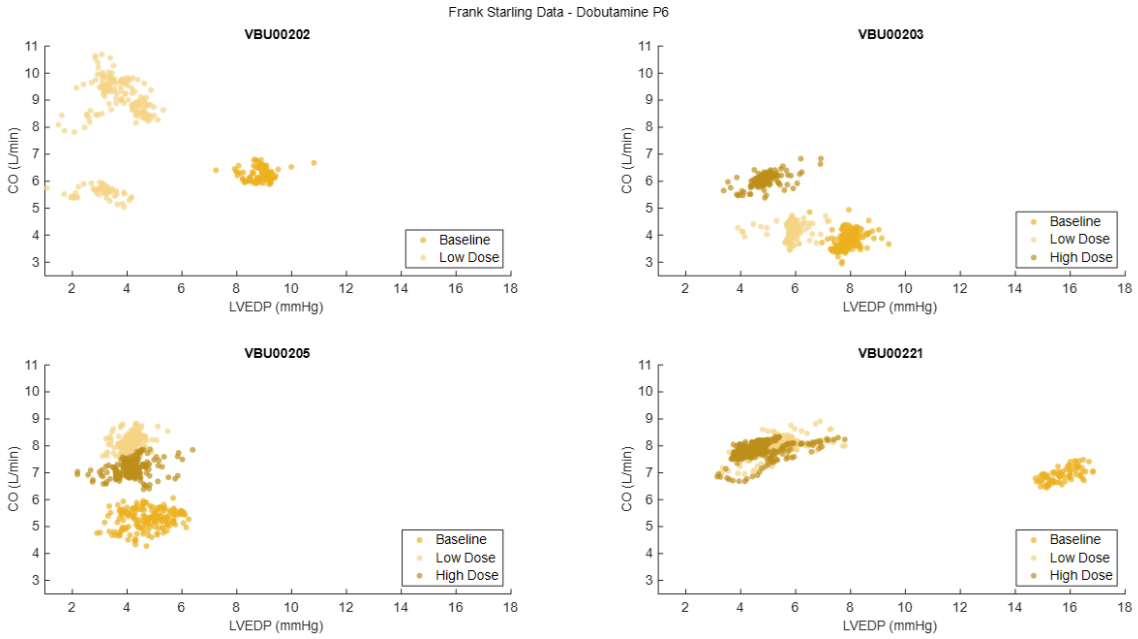

Figure B-5: Frank-Starling representation of dobutamine at P-6 across all animals

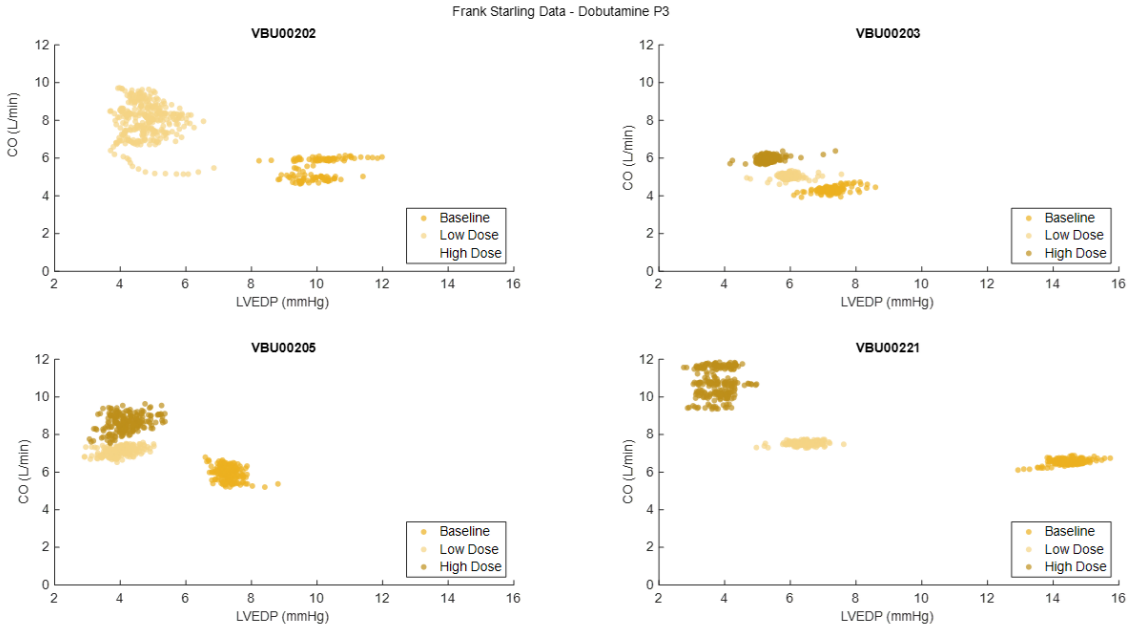

Figure B-6: Frank-Starling representation of dobutamine at P-3 across all animals

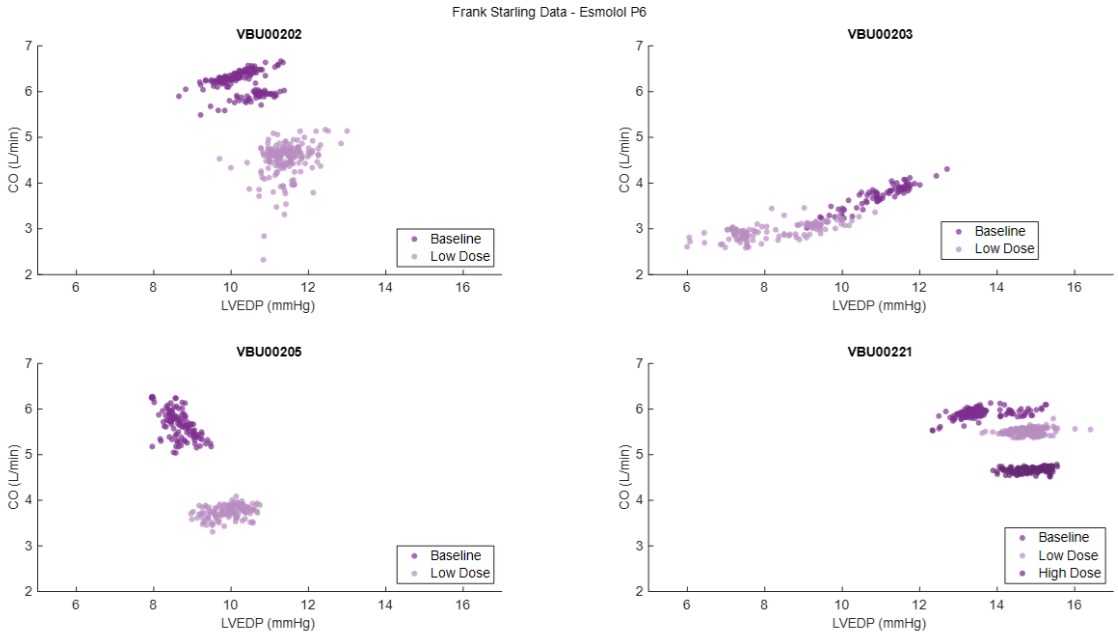

Figure B-7: Frank-Starling representation of esmolol at P-6 across all animals

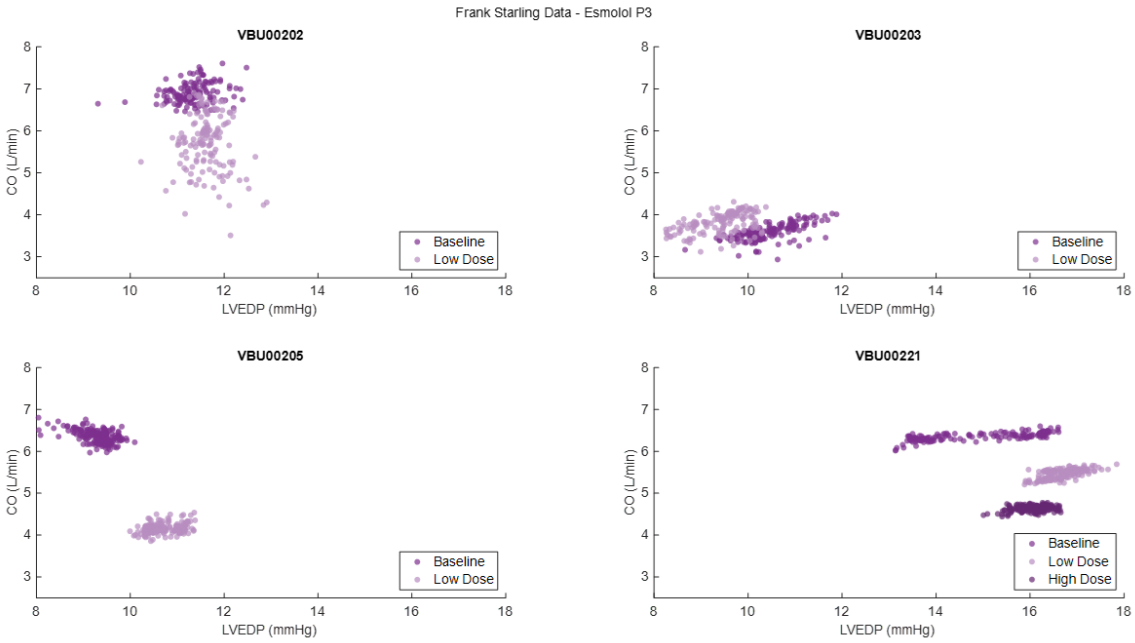

Figure B-8: Frank-Starling representation of esmolol at P-3 across all animals